# 4.5GHz LOW NOISE AMPLIFIER

Submitted By

VARGHESE GEORGE

In partial fulfilment of the requirements for the M.Tech Degree

in

ELECTRONICS ENGINEERING

AT

COCHIN UNIVERSITY OF SCIENCE AND TECHNOLOGY

Guided By

Prof N.V.G SARMA

MMW LAB

RAMAN RESEARCH INSTITUTE

BANGALORE

COCHIN UNIVERSITY OF SCIENCE AND TECHNOLOGY

KOCHI 682022

# RAMAN RESEARCH INSTITUTE

PROF. N.V.G. SARMA
Professor & Head
Millimeterwave Laboratory

27th May 1993

## CERTIFICATE

This to certify that the project work titled "4.5 GHz Low Noise Amplifier" was carried out by Mr. Varghese George in the Millimeterwave Laboratory of the Raman Research Institute, Bangalore under my guidance for the partial fulfilment of the requirements for the award of Master of Technology degree in Electronics Engineering of Cochin University of Science and Technology, Cochin.

N.V.G. Sarma
(N.V.G. SARMA)

Address:
C.V. Raman Avenue
Sadashivanagar
Bangalore 560 080, INDIA

Tel: (812) 340122
Fax: (812) 340492

Telex: 845 2671 RRI IN
Telegrams: RAMANINST

# COCHIN UNIVERSITY OF SCIENCE AND TECHNOLOGY

KOCHI 682022

## *CERTIFICATE*

*This is to certify that this thesis work entitled 4.5GHz LOW NOISE AMPLIFIER has been sucessfully completed by VARGHESE GEORGE as a partial fulfilment of the M.Tech degree in Electronics engineering during the year 1992-1993 in the department of electronics at Cochin University of Science and Technology.*

N-V-G Sarma

Guide

Prof. N.V.G Sarma

Head of the Department

DR. K.G Nair

## Abstract

A Low Noise Amplifier for Radio Astronomy purposes operating at 4.5GHz is made. A completely planar structure is opted for, except the active device and the coupling capacitors. A gain of 11dB and noise temperature of 55K is obtained with a single stage. Based on the single stage design a three stage amplifier is constructed with a gain of 29dB and noise temperature of 45K with 1GHz bandwidth. The amplifier made is conditionally stable.

Further optimization can be done to the circuit to improve the stability as well as the noise and gain performance.

# ACKNOWLEDGEMENT

I am thankful to the Director, Raman Research Institute, Bangalore, for allowing me to do my thesis work at the Millimeter Wave Laboratory. This work was made possible only because of the guidance of Prof. N.V.G.Sarma at the Raman Research Institute. I am extremely thankful to Ms. Seethalakshmi at the MMW lab, RRI, without whose help this work would not have reached this level of completion. The experience of Sadik in this field was a great help to me. I am grateful to everyone in the MMW Lab who have helped me in this work.

I wish to thank the people at the Precision Workshop for their prompt and excellent work.

I also wish to thank Prof. K.G.Nair , Department of Electronics, C.U.S.A.T., for his help .

# Contents

# Chapter 1

# INTRODUCTION

The science of Radio Astronomy has its beginnings in the experiments of Karl G Jansky in 1931. This branch of astronomy has to deal with signal strengths which are very low compared to the background noise level. The sensitivity or minimum detectable temperature is determined by the output fluctuations due to the statistical nature of the noise waveform, which is given by,

$$\Delta T_{rms} = \frac{K_s * T_{sys}}{\sqrt{B * T * n}} \tag{1.1}$$

where,

$T_{rms}$ = rms system noise temperature, K

$K_s$ = sensitivity constant, dimensionless

$T_{sys}$ = system temperature, K

B = predetection bandwidth, Hz

T = post detection integration time, sec

n = number of records averaged, dimensionless

The noise level can be reduced either by reducing $T_{sys}$, or increasing the integration time, or increasing the predetection bandwidth, or by taking the average of more than one observation. Increasing the integration time beyond a point distorts a true source profile. Increasing the predetection bandwidth results in a loss of spectral information. This leaves the option of reducing the system temperature, which

is dependent on the antenna temperature and the receiver temperature.

The antenna temperature depends on the region at which it is pointed, stray pickup due to the side lobes and the general antenna design. Hence, for a given antenna the only option to improve the system sensitivity is to reduce the receiver temperature.

The Low Noise Amplifier which has been developed is to be used in the receiver system of the Radio Telescope at the Raman Research Institute(RRI), Bangalore. The radio telescope at RRI works in the 80Ghz to 115Ghz band. Some of the transitions of 12CO, 13CO, SiO, etc occur in this band and gives important Radio Astronomical information. The strength of the signals detected at RRI is in the range of 0.1K to 40K.

The basic system setup is as shown in figure 1.1. The front end is a mixer which is used to downconvert the frequency. The IF has been chosen as 4.5Ghz. The amplifier developed will be modified to a cooled amplifier and used as the IF amplifier.

The technology available to obtain the low noise required is as shown in the figure 1.2. Parametric amplifiers and masers dominated this field in the last decade. They are complex, offer a very narrow band width and combined with the fact that they require pump sources make them unsuitable for use in a receiver system.

Transistors are emerging as replacements giving comparable performance. Bipolar Transistors were the first choice which then gave way to Field Effect. FETs are being surpassed in performance by High Electron Mobility Transistors(HEMT). HEMTs make use of two dimensional electron flow to achieve low noise. PHEMTs which are modifications of HEMTs have been reported to give noise temperatures of the order of a few degrees kelvin under cooled conditions.

In this project PHEMTs are used to develop a three stage amplifier. A single stage is developed first and based on the results a three stage is developed to give a gain of 30dB and a noise of 50K over the 4GHz-5GHz band at room temperature. A planar structure employing distributed passive components is aimed for, while

retaining the capability of tuning.

Chapter Two deals with the circuit theory.

Chapter Three deals with device theory of HEMTs.

Chapter Four gives the Amplifier design procedure.

Chapter Five discusses the measurement procedure and the setup.

Chapter Six gives the results obtained with the single stage and the final three stage and conclusions.

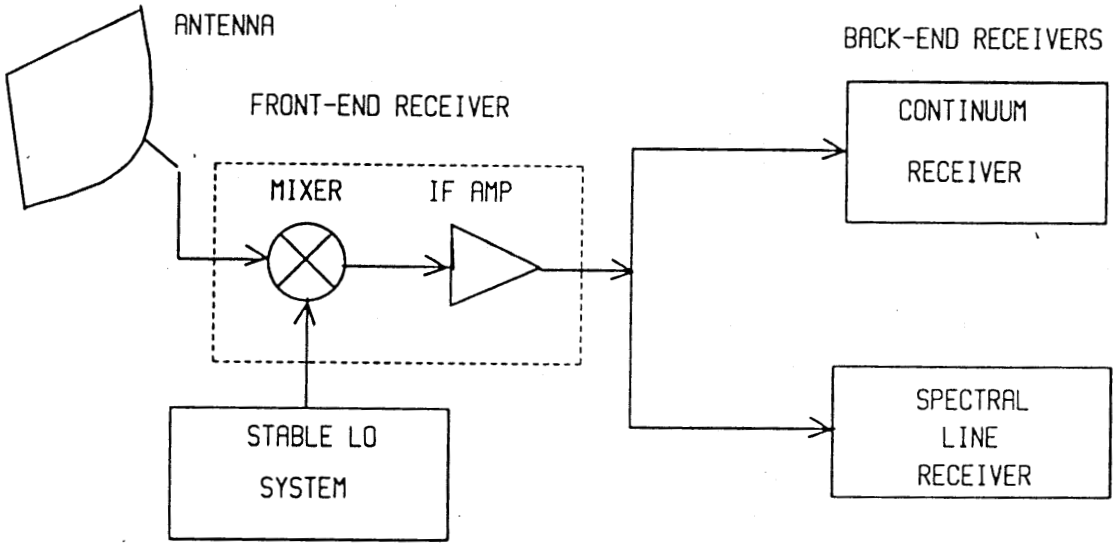


FIG. 1.1 BASIC RECEIVER SYSTEM

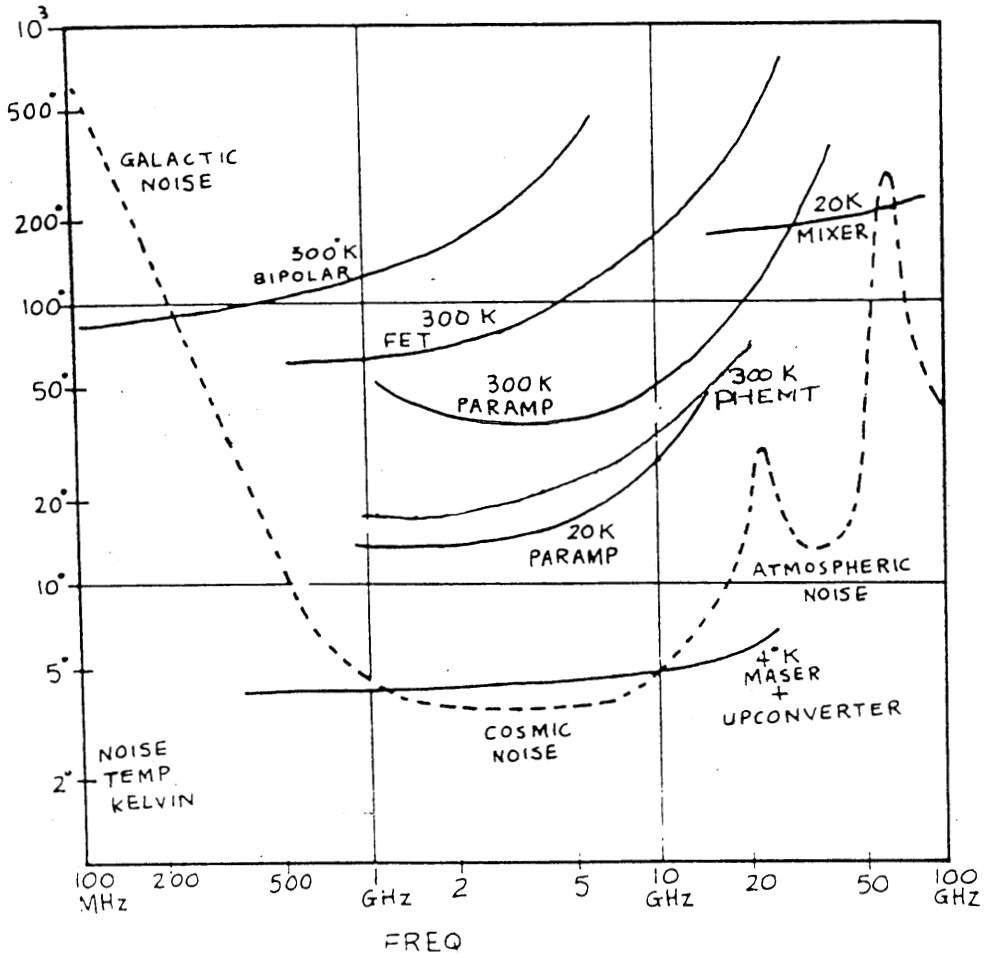


FIG 1.2 TECHNOLOGY AVAILABLE FOR LOW NOISE

# Chapter 2

# CIRCUIT THEORY

In this chapter basic circuit theory pertaining to amplifier design will be discussed. Scattering parameters, noise theory, and stability of two port networks will be dealt with. Scattering parameters are basically a means of characterization of n-port networks and plays an important role in amplifier design. The noise temperature of a two port network is an important factor in low noise amplifier design and has to be studied in detail. Stability of a two port network means the difference between success and failure in amplifier design.

## 2.1 S Parameters:

The scattering or S-parameters are used for n-port network characterization. It's advantages over h, y and z parameter sets are obvious at higher frequencies. These parameter sets relate total voltages and currents at each of the two ports. At higher frequencies the problems faced by the h, y and z parameter network characterization are as follows :

1. Short and open circuits are difficult to achieve over a broad band of frequencies.
2. Equipment not readily available to measure total voltage and total current at the ports of the network.

3. Active devices like transistors and tunnel diodes are not always open and short circuit stable.

In S-parameter characterization these problems are overcome and traveling waves are used as variables.

Voltage, current and power can be considered to be waves traveling in both directions along a transmission line. If we insert a two port network into the transmission line we have traveling waves that are interrelated. In fig 2.1 we see that $E_{r2}$ is made up of that portion of $E_{i2}$ that is reflected from the output port and the portion of $E_{i1}$ that is transmitted through the network. All the other waves are also made up in a similar fashion. These traveling waves can be related. Starting from the h-parameter set we have,

$$V_1 = h_{11}I_1 + h_{12}V_2 \tag{2.1}$$

$$I_2 = h_{21}I_1 + h_{22}V_2 \tag{2.2}$$

where,

$$V_1 = E_{i1} + E_{r1} \tag{2.3}$$

$$V_2 = E_{i2} + E_{r2} \tag{2.4}$$

$$I_1 = \frac{E_{i1} - E_{r1}}{Z_0} \tag{2.5}$$

$$I_2 = \frac{E_{i2} - E_{r2}}{Z_0} \tag{2.6}$$

$Z_0$ is defined as the characteristic impedance of the line .

Substituting eqt.s 2.3 , 2.4 , 2.5 and 2.6 in eqts. 1.1 and 1.2 and rearranging, we get,

$$E_{r1} = f_{11}(h)E_{i1} + f_{12}(h)E_{i2} \tag{2.7}$$

$$E_{r2} = f_{21}(h)E_{i1} + f_{22}(h)E_{i2} \tag{2.8}$$

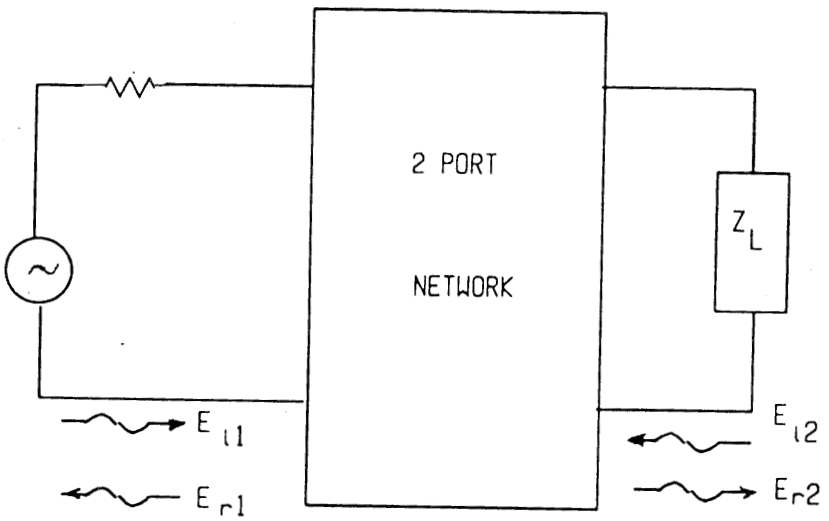


FIG. 2.1 TRAVELING WAVE CONCEPT IN 2 PORT NETWORK.

Here it is seen that $f_{11}$ , $f_{12}$, $f_{21}$, $f_{22}$ represent a new set of network parameters relating the traveling voltage waves. Eventhough here they are represented in terms of h parameters they can be derived from any of the network parameters.

Dividing both sides of eqt.s 2.7 and 2.8 by $\sqrt{Z_0}$ , the characteristic impedance of the transmission line , and defining new variables ,

$$a_1 = \frac{E_{i1}}{\sqrt{Z_0}} \tag{2.9}$$

$$a_2 = \frac{E_{i2}}{\sqrt{Z_0}} \tag{2.10}$$

$$b_1 = \frac{E_{r1}}{\sqrt{Z_0}} \tag{2.11}$$

$$b_2 = \frac{E_{r2}}{\sqrt{Z_0}} \tag{2.12}$$

we get,

$$b_1 = S_{11}a_1 + S_{12}a_2 \tag{2.13}$$

$$b_2 = S_{21}a_1 + S_{22}a_2 \tag{2.14}$$

We can see that the new variables have the dimension of power and these traveling waves can be called as traveling power waves. This can be represented using a signal flow graph as in fig 2.2. Two port networks were discussed so far, the same concept is valid for the characterization of n-port networks as well . For an n-port network the S-parameters are given by,

$$\begin{vmatrix} b_1 \\ b_2 \\ \vdots \\ b_N \end{vmatrix} = \begin{vmatrix} S_{11} & S_{12} & \dots & S_{1N} \\ S_{21} & S_{22} & \dots & S_{2N} \\ \vdots & \vdots & \dots & \vdots \\ S_{N1} & S_{N2} & \dots & S_{NN} \end{vmatrix} \begin{vmatrix} a_1 \\ a_2 \\ \vdots \\ a_N \end{vmatrix} \tag{2.15}$$

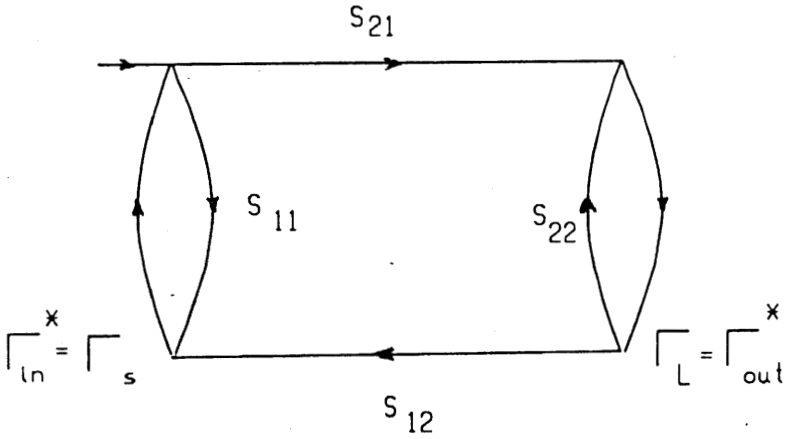


$\Gamma_{in}$ = Input reflection coefficient

$\Gamma_{s}$ = Source reflection coefficient

$\Gamma_{L}$ = Load reflection coefficient

$\Gamma_{out}$ = Output reflection coefficient

FIG. 2.2 SIGNAL FLOW GRAPH REPRESENTATION OF 2 PORT S PARAMETERS.

## 2.2 Noise Theory:

In a receiving system the components degrade the signal to noise ratio (SNR) of the signal passing through. A figure of merit is assigned to the components and to the system as a whole so as to optimize the performance. This figure of merit is Noise Figure and is defined as ,

$$NoiseFigure = \frac{Input\ SNR}{Output\ SNR} \tag{2.16}$$

$$= \frac{S_i/N_i}{S_o/N_o} \tag{2.17}$$

taking,

$$S_o = GS_i \tag{2.18}$$

$$F = \frac{N_o}{N_iG} \tag{2.19}$$

$$= \frac{N_o/G}{N_i} \tag{2.20}$$

$$= \frac{Output\ noise\ referenced\ to\ the\ input\ port}{input\ noise} \tag{2.21}$$

Where,

$S_i$ = input signal strength

$S_o$ = ouput signal strength

$N_i$ = noise strength at the input

$N_o$ = noise strength at the output

G = Gain of the system

This expression is independent of the signal. The total noise at the output is due to the input noise and the noise contributed by the system.

By Nyquist theorem the noise power generated by a resistive termination due to the random motion of thermally agitated electrons is given by,

$$P = kTB \tag{2.22}$$

Where,

T = termination temperature , K

k = Boltzman's constant , 1.38 * $10^{-23}$ Joules/K

B = bandwidth , Hz

Substituting in eqt. 2.20,

$$F = \frac{N_o}{kT_oBG} \tag{2.23}$$

The noise added by the system is given by,

$$N_S = N_o - kT_oBG \tag{2.24}$$

$$= (F-1)kT_oBG \tag{2.25}$$

This equation gives rise to a useful conceptual model given in Fig.2.3. This consists of a resistive termination, $(F-1)kT_oB$ at the input to an ideal receiver of gain G and 0dB Noise figure. This also gives rise to another useful concept of effective noise temperature, where the receiver noise can be attributed to a resistive load at the temperature given by,

$$T_e = (F-1)T_o \tag{2.26}$$

Thus, for any noise figure, F, we can introduce an equivalent noise temperature, $T_e$, which represents the temperature of a matched termination that gives rise to the amount of added noise at the output of the system equivalent to the non-ideal receiver. This temperature is referred to the receiver input terminals. The temperatures of the components can be added to give the overall system performance.

## 2.3 Stability Considerations :

For obtaining optimum gain and noise performance out of the transducer, we terminate the input and output ports of the transducer with designed matching circuits.

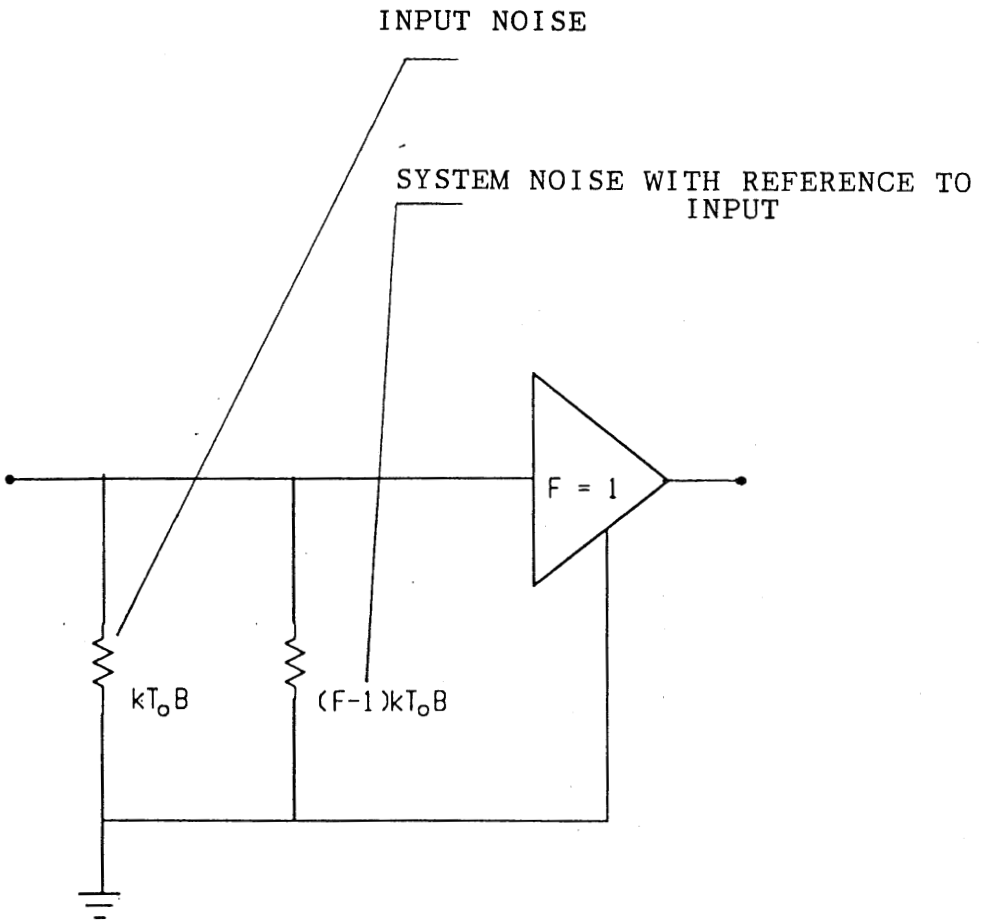


FIG. 2.3 CONCEPTUAL MODEL OF NOISE FIGURE

At this juncture we have to ascertain that the transducer is stable for that input and output impedance termination. Depending on this a network can be described as conditionally or unconditionally stable.

A network is said to be conditionally stable if the real part of the input impedance ($Z_{in}$) and output impedance ($Z_{out}$) is greater than zero for some positive real source and load impedances at a specific frequency.

A network is unconditionally stable if the real part of $Z_{in}$ and $Z_{out}$ is greater than zero for all positive real source and load impedances at a specific frequency.

That is the input reflection coefficient ($\Gamma_{in}$) and the output reflection coefficient ($\Gamma_{out}$) must be less than or equal to one. Based on these criteria the K factor of a two port network is derived giving,

$$K = \frac{1 + \mid S_{11}S_{22} - S_{12}S_{21} \mid^2 - \mid S_{11} \mid^2 - \mid S_{22} \mid^2}{2 * \mid S_{12} \mid\mid S_{21} \mid} > 1 \tag{2.27}$$

The stability has to be found out over the frequency region of interest.

## 2.4 Stability Circles:

The input and output reflection coefficients are given by,

$$\Gamma_{in} = S_{11} + \frac{S_{21}S_{12}\Gamma_L}{1 - S_{22}\Gamma_L} \tag{2.28}$$

$$\Gamma_{out} = S_{22} + \frac{S_{21}S_{12}\Gamma_S}{1 - S_{11}\Gamma_S} \tag{2.29}$$

where,

$\Gamma_L$ = load reflection coefficient

$\Gamma_S$ = source reflection coefficient

By setting $\Gamma_{in}$ equal to one we obtain a boundary with $\Gamma_{in}$ greater than one on one side and less than one on the other side.The solutions for $\Gamma_L$ will lie on a circle whose radius and center are given by,

$$radius = r_L = \left| \frac{S_{12}S_{21}}{| S_{22} |^2 - | \Delta |^2} \right| \tag{2.30}$$

$$center = C_L = \frac{(S_{22} - \Delta S_{11}^*)^*}{| S_{22}^2 - | \Delta |^2} \tag{2.31}$$

where,

$$\Delta = S_{11}S_{22} - S_{21}S_{12} \tag{2.32}$$

The circle plotted on a smith chart will be as shown in fig 2.4 and one side of the circle will represent the stable region and the other side the unstable region. With $S_{11} < 1$ the region inside the circle is the unstable region. Hence, we need to be careful that $\Gamma_L$ falls outside the stability circle. For $S_{11} > 1$ the converse is true.

To ensure that the network is unconditionally stable at a given frequency we must be able to terminate the input and output ports with any passive load without moving into an unstable condition. This means that the stability circle must be completely outside the smith chart and the region outside the stability circle represents the stable operating region. To satisfy this requirement we must ensure the following,

$$|| C_S | - r_S | > 1 \tag{2.33}$$

$$| S_{22} | < 1 \tag{2.34}$$

$$|| C_L | - r_L | > 1 \tag{2.35}$$

$$| S_{11} | < 1 \tag{2.36}$$

For the network these conditions must be satisfied in the whole frequency band of interest.

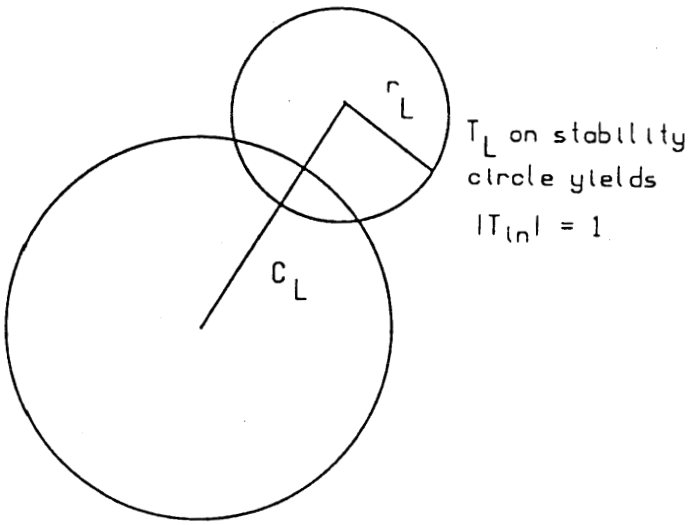


FIG. 2.4 OUTPUT STABILITY CIRCLE

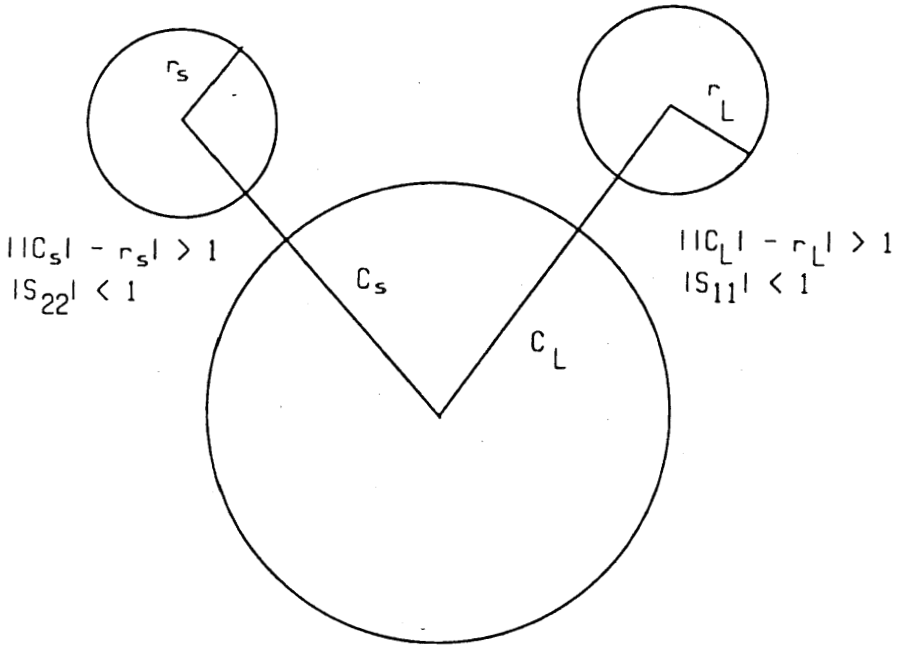


FIG. 2.5 STABILITY CIRCLES FOR UNCONDITIONAL STABILITY

# Chapter 3

# DEVICE THEORY

Silicon bipolar transistors which were used initially in microwave circuits gave way to Metal Semiconductor Field Effect Transistor (MESFETs) as the preferred device for low noise microwave designs. These are also being replaced by hetrojunction devices. During the last decade advances in the technology of III-V compound semiconductors have resulted in the fabrication of practical heterojunction devices which make use of the properties of the junctions between materials of differing energy gaps for their operation. In this area there are two devices of interest for microwave applications, the Heterojunction Bipolar Transistor (HBT) and the High Electron Mobility Transistor(HEMT). The HEMTs are also known by the names of Two Dimensional Electron Gas FET(TEGFET) and Modulation doped FET(MODFET). We are interested in the structure of HEMTs, operation principle which is responsible for the low noise, characterization, and properties under cryogenic cooling.

## 3.1 Heterojunction:

The existence of electron accumulation layer at the interface of certain heterojunctions was first proposed by Anderson. When a heterojunction of Ge on GaAs is formed in which the narrow band gap material has a higher electron affinity than the wide band gap material, electrons are attracted to the low band gap material

and accumulate at the interface. This finding was followed by the modulation doped GaAs/AlGaAs superlattice in which the donor impurities were there only in the wide bandgap AlGaAs layer (Fig.3.1). This resulted in higher mobility because of the reduced donor impurity scattering in the GaAs layer. The electrons are confined to a two dimensional sheet at the interface. Hence, the motion of the electrons are restricted to two dimensions and this explains the reduction in noise due to the reduced randomness in motion.

To form high quality hetrostructure, it is often necessary to have a semiconductor pair with similar lattice parameters. When this happens the hetrostructure is said to be lattice matched. Hetrostructures are often formed by growing ternary alloys on binary alloys with properly chosen composition to provide lattice matching, and more important, desired energy gap and band offset.

## 3.2 Modulation Doped Heterojunction:

By modulation doping the coulombic interaction, known as ionized impurity scattering can be reduced. An AlGaAs/GaAs hetrojunction can be grown with the n-type donors introduced only into the wide bandgap AlGaAs. Since the GaAs has the lower energy the electrons diffuse from the AlGaAs conduction band to the GaAs conduction band. The depleted AlGaAs layer forms a positively charged region which attracts the electrons back to the interface. The resulting electric field perpendicular to the interface results in severe band bending as shown in Fig.3.2. Electron in the 2 Dimension Electron Gas (2DEG) are confined to a triangular potential well at the heterojunctin as shown. The band diagram in Fig.3.2 includes an undoped spacer layer at the interface. These spacer layers improve the mobility at the interface by reducing the scattering due to donors in the doped AlGaAs layer.

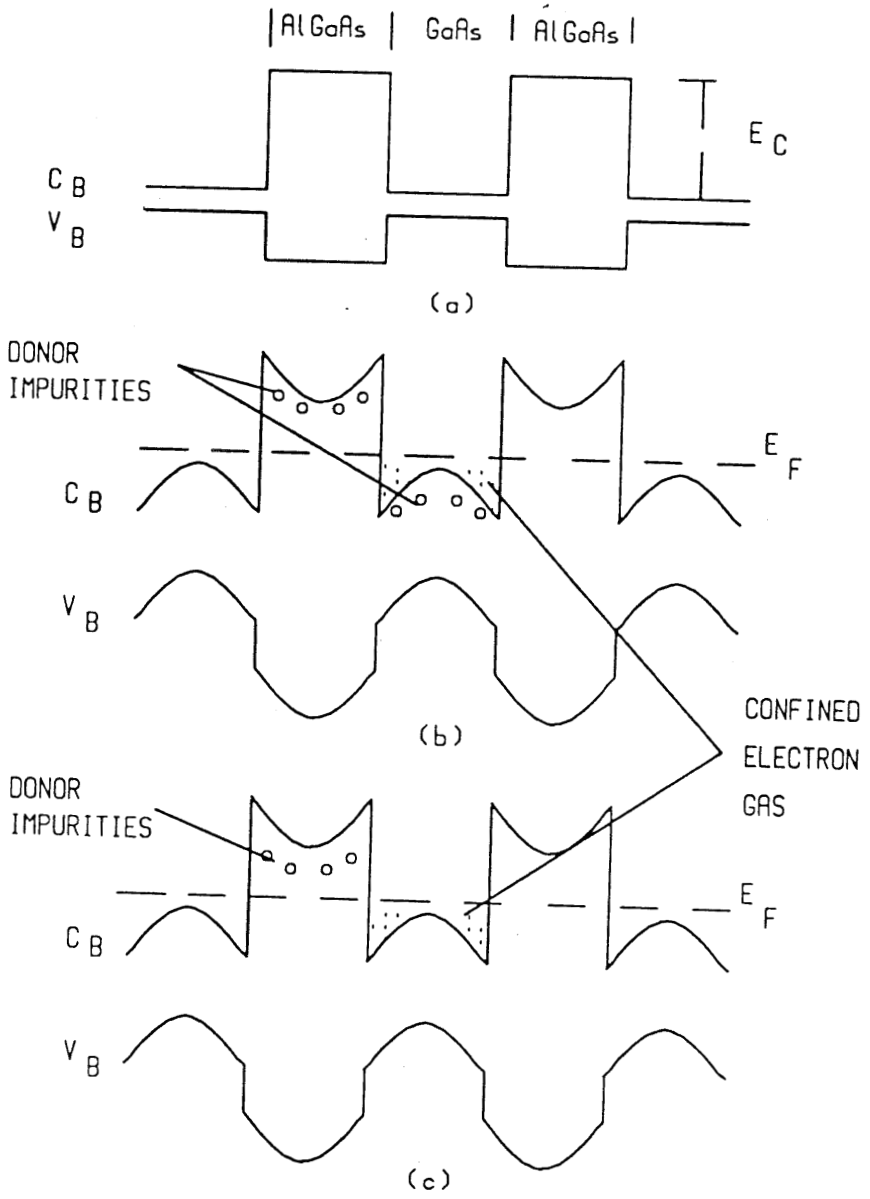


FIG. 3.1 ENERGY BAND DIAGRAM FOR (a) UNDOPED, (b) UNIFORMLY DOPED AND (c) MODULATION DOPED.

GaAs/AlGaAs SUPERLATTICE [3]

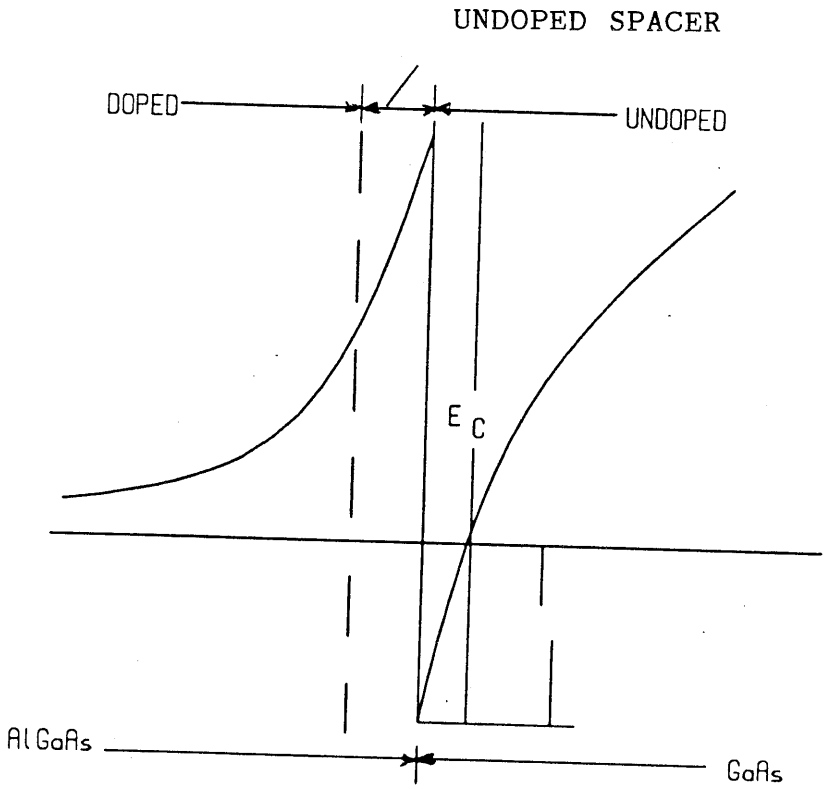


FIG. 3.2 CONDUCTION BAND DIAGRAM OF A SINGLE INTERFACE MODULATION DOPED HETEROJUNCTION.

### 3.2.1 Transport Properties:

Enhanced transport properties are critical in the operation of the HEMT and affect material design for optimized performance. Other than the ionized impurity scattering there are other mechanisms which limit the mobility in the heterojunction interface. Principal among them is the bulk phonon interactions, both acoustical and optical which cannot be avoided at finite temperatures. At temperatures above 80K the mobility data of the modulation doped structures is of the same order as that of highly pure GaAs (8500- 9000 $cm^2$/V-s). This sets a limit to the highest obtainable mobility in modulation doped structures a 300K. At low temperatures due to the reduced phonon scattering there is a dramatic increase in the mobility in modulation doped structures.

Other than phonon scattering the other scattering mechanisms are given below,

**Ionized impurity scattering:** The ionized impurity scattering due to the remote impurities in GaAs and the doped AlGaAs is the main reason for scattering at low temperatures. Eventhough the mobility increases with increase in spacer layer thickness it has been reported that a peak in mobility is reached at a spacer layer thickness of 50-100Å. This can be explained in the light of the result that the sheet carrier concentration in the 2DEG reduces with the increase in the spacer layer thick ness.

**Interface Roughness Scattering:** Though direct evidence of the dependence of mobility on interface roughness is not available, indirect evidence is available. It is reported that optimum mobilities are obtained at crystal growth temperature between $600°C$ and $700°C$. This temperature range coincides with the temperature range over which the interface roughness in superlattices of GaAs/AlGaAs has been found to be the lowest.

**Inter-Sub-Band Scattering:** Due to the quantization of the 2DEG potential well, a number of sub-bands exist which represent discrete electron energy states. As the carrier sheet concentration is increased, states in the lowest sub-band

become filled and eventually states within the first excited sub-band become available for scattering resulting in a decrease in the mobility. Theoretical predictions give a decrease in mobility when the sheet carrier concentration increases above $7 * 10^{11}/cm^2$ and then it increases again ultimately.

## 3.3 HEMT Structure:

A typical epitaxial structure required for the conventional HEMT is shown in Fig.3.3. The material properties that must be optimized for controlling 2DEG density and transport properties are:

- Quality of the heterointerface, which includes, interface abruptness, interface smoothness and freedom from interface states.
- Ionized impurity density in the undoped GaAs drift layer.
- Density of donors in the doped AlGaAs/GaAs layer that can contribute to electrons in the 2DEG.

To maximize the sheet density at of the 2DEG the following methods are used.

- Maximizing conduction band discontinuity.
- Maximizing the shallow donor density in the AlGaAs layer.
- Minimizing the spacer layer thickness.

The topmost layer in the conventional HEMT structure is $n^+$GaAs. This is for providing good ohmic contacts and for reducing the parasitic source resistance.

The doping density and thickness of the AlGaAs layer are adjusted to obtain the desired threshold voltage and enhancement or depletion mode devices. For proper device performance the layer thickness has to be controlled to within 11Å. With the current development of production technology only Molecular Beam Epitaxy (MBE) process can attain this accuracy. MBE grown layers suffer from surface defects,

called oval defects which result in the shifting of device parameters. Another growth technology, Metal Organic Chemical Vapor Deposition (MOCVD) has recently been successful in obtaining MBE accuracy and has the additional advantage of being free from surface defects.

The HEMT technology is in a very rapidly evolving state, techniques are being developed to improve upon the conventional HEMT, and new device structures are evolving. Table 3.1 gives some of the variants of conventional HEMT. Principal among these is the Pseudomorphic HEMT (PHEMT) which gives a better performance in power added efficiency, noise figure, gain, reliability, and input power requirements as compared to conventional HEMTs.

## 3.4 Pseudomorphic HEMT:

Pseudomorphic HEMTs (PHEMT) are a modification of HEMTs. Here, a thin layer of narrow bandgap InGaAs, which is lattice mismatched with GaAs ($\sim$ 1%) is sandwiched between an undoped GaAs buffer and a doped GaAs cap layer. The InGaAs is thin enough ($\sim$ 200 Å) that the lattice strain is taken up coherently by this quantum well resulting in a dislocation free pseudomorphic material.

The conduction band discontinuity or the discontinuity between the donor level in the high bandgap material and the narrow bandgap conduction band is an important consideration in any modulation doped system. The major effects of a small discontinuity are,

- Less efficient electron transfer and hence a smaller 2DEG concentration.
- Compounds the problem of parasitic MESFET effect.
- Increased possibility of hot electron injection to the high band gap material.

In the GaAs/AlGaAs system to provide a $\Delta E_c$ sufficient enough to minimize these effects, an Al mole fraction greater than 0.2 is required. In an InGaAs/AlGaAs system a mole fraction of only 0.15 is required for a $\Delta E_c$ of 0.3eV. The use of high

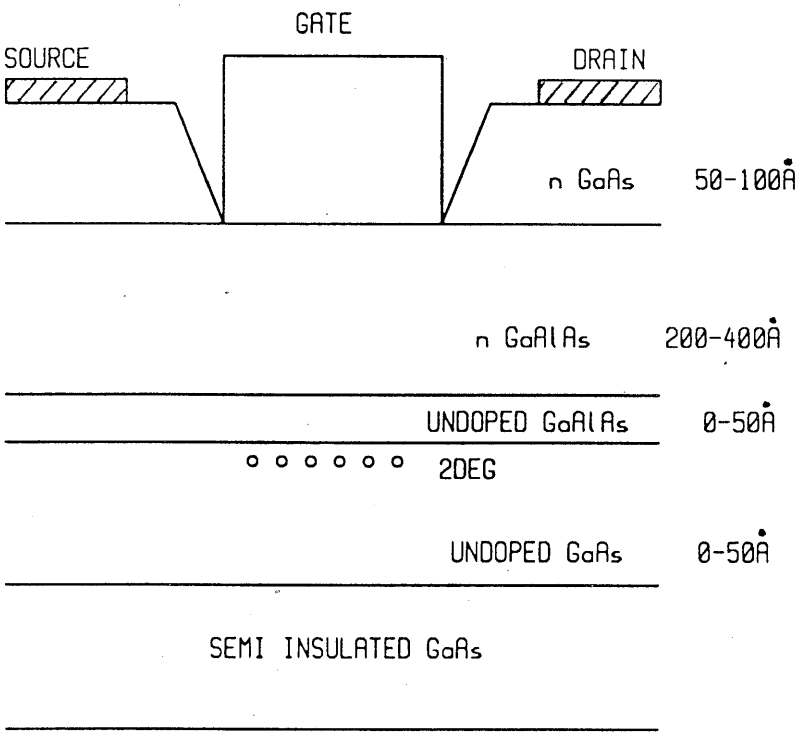


FIG. 3.3 CONVENTIONAL HEMT STRUCTURE.

mole fraction ($\geq 0.2$) can lead to persistent photoconductivity and collapse of I-V characteristics if AlGaAs is not grown under optimum conditions.

In micrometer and sub micrometer structures the intrinsic transconductance is determined to first order by the product of average electron velocity and the 2DEG capacitance. A high transconductance is expected with InGaAs based system over GaAs due to the high saturation velocity in InGaAs. The 2DEG capacitance can be made high by decreasing the thickness and increasing the doping concentration of the higher band gap material. The transconductance in InGaAs MODFET may also be superior because of a smaller average distance of the 2DEG from the interface due to the improved carrier confinement in the quantum well.

The improved saturation velocity in the InGaAs should also result in a significant increase in the cut off frequency given by,

$$f_T = \frac{V_{avg}}{2\pi L_g} \tag{3.1}$$

where,

$V_{avg}$ = average electron velocity under the gate

$L_g$ = gate length

The generation recombination noise is also expected to be considerably lower due to a reduction of occupied deep levels in low mole fraction AlGaAs.

## 3.5 Equivalent Circuit:

The small signal equivalent circuit of the HEMT closely resembles that of the MESFET. It is described in Fig.3.4. The intrinsic device circuit is represented inside the dashed rectangle. The parasitic access elements are represented outside the rectangle. The values of the elements in the equivalent circuit can be obtained by number of methods.

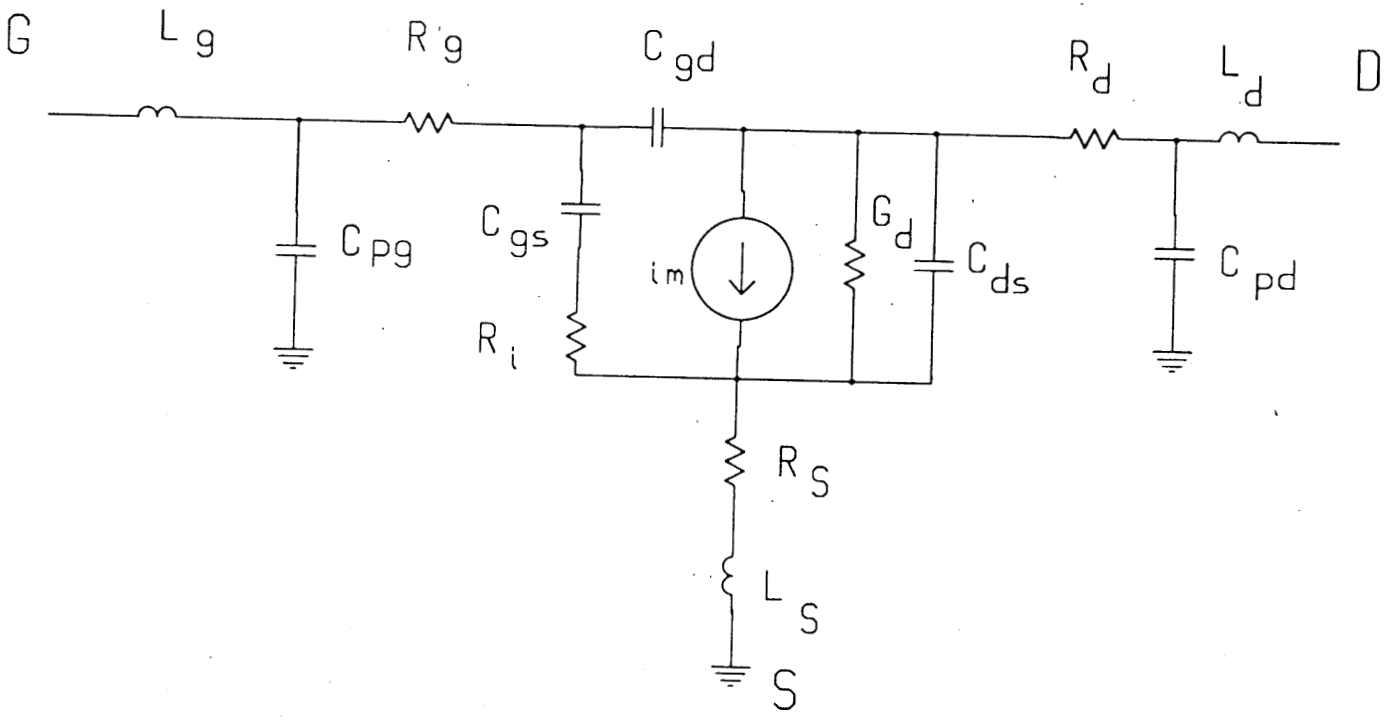


FIG.3.4 HEMT EQUIVALENT CIRCUIT

## 3.6 Parametric Analysis:

The important device figures which are analyzed as a function of the device parameters are, noise figure, cut-off frequency and gain [4].

The noise figure of a HEMT device can be written as

$$NF = 1 + k_f * \frac{f}{f_T}\sqrt{G_m(Rs + R_g)} \tag{3.2}$$

where,

$k_f$ = form factor (1.6 for HEMT)

f = operating frequency

$f_T$ = cut off frequency

$G_m$ = intrinsic transconductance of the 2DEG layer

$R_s$ = source resistance

$R_g$ = gate resistance

The cut-off frequency is given by,

$$f_T = \frac{G_m}{2\pi C_{gs}} = \frac{V_{avg}}{2\pi L_g} \tag{3.3}$$

where,

$C_{gs}$ = gate to source capacitance

$L_g$ = gate length

from eqt 3.2 and 3.3

$$NF = [1 + k_f * 2\pi C_{gs}\sqrt{\frac{(Rs + Rg)}{G_m}} \tag{3.4}$$

It is seen from the above equations that the basic requirements for low noise performance are high $f_T$, low values of $C_{gs}, R_s$ and $R_g$.

The maximum gain of the device is given by,

$$G_{max} = \frac{f_T^2}{f} \tag{3.5}$$

It is seen that a higher cut-off frequency is required for high gain and low noise performance. This in turn is dependent on the saturation velocity in the 2DEG. The saturation velocity is greater in a PHEMT ($3.6 * 10^{17} cm/sec$) as compared to the conventional HEMT ($2.67 * 10^{7} cm/sec$).

## 3.7 Cryogenic Temperature Properties:

Due to the improvement in device transport properties the device performance can improve at low temperatures ($< 100$K). But, problems of drain current collapse, persistent photoconductivity and threshold voltage shift can reduce the usefulness. Unusual distortion of the I-V characteristic or oscillations caused mainly by the Gunn type instabilities in GaAs are also present.

The shift in the threshold voltage ($\sim 0.2V$) is attributed to the trapping by the DX centers (deep electron levels) of the hot carriers in AlGaAs resulting in a 2DEG concentration reduction. This can be alleviated by illumination with white light. The DX centers which are effectively empty at room temperature tend to fill up at low temperature. Illuminating the device empties the traps and these excited electrons are not readily recaptured due to a large potential barrier to capture leading to a persistent photoconductivity. These DX traps have been attributed to a high mole fraction of Al ($\sim 0.2$) in the AlGaAs layer. In PHEMTs the mole fraction required is low as compared to HEMTs and these degradation due to DX traps are eliminated.

| *Salient Features or Name* | *Description* |
|---|---|
| Graded (Al,Ga)As layer | (Al,Ga)As donor layer graded in composition from (Al,Ga)As at 2DEG interface to GaAs at cap interface to facilitate ohmic contact formation. |
| Inverted HEMT structure | Undoped GaAs drift layer grown on top of doped (Al,Ga)As layer. |
| Multiple Heterojunction HEMT | Epitaxial layer structure with more than one heterointerface providing electrons to the 2DEG. |
| Planar doped layer | Doping of the donor layer confined to a single atomic layer. |
| Quantum well drift layer | Thin (300-400Å) low bandgap drift region confined on both sides by potential barrier formed by heterojunction with higher bandgap materials. |
| Superlattice buffer layer | Buffer layer composed of undoped (AlGa)As/GaAs layers. |
| Superlattice donor layer | Superlattice donor layer (eg; (AlGaAs)/GaAs with doping confined to GaAs). |
| Pseudomorphic HEMT | Drift region comprising low bandgap, high mobility layer, not lattice matched to donor layer. |
| (Al,In)As/(Ga,In)As/InP HEMT | Lattice matched HEMT epitaxial layer with (Al,In)As donor layer and (Ga,In)As drift layer on semi-insulating InP substrate. |
| HEMT on Si substrate | HEMT epitaxial layer grown on a Si substrate. |
| Heterostructure insulated gate FET (HIGFET) | No donor layer, 2DEG induced in a channel by varying gate electrode potential, similar to MOSFETs. |
| p-channel HEMT | Donor layer doped with Be to provide a 2DEG hole gas at interface. |

Table 3.1: Variations to basic HEMT structure

# Chapter 4

# AMPLIFIER DESIGN

The complete design and assembly of the single stage amplifier and the three stage amplifier is discussed in this chapter. The impedance matching circuits are designed using microstrip transmission lines and a completely planar structure is aimed for. Initially the single stage is designed and tested with the transistors which are to be used in the final three stage. Based on this the three stage is designed and tested.

In the design process, matching for noise is an important criterion. Usually matching for optimum noise and gain simultaneously is not possible without feedback. The bias circuitry is important and must prevent any ac from entering the amplifier matching circuit. Any oscillations entering through the bias can make the amplifier unstable.

## 4.1 Radial Stub:

Radial stubs are an alternative to rectangular open and short circuit stubs in microwave circuits. They offer solutions to requirements of well defined low impedance levels and broad band width. In rectangular stubs the line widths at higher frequencies place a limitation on the low impedances available. Radial stubs maintain the lower impedance level over a wider range than rectangular stubs, Giannini[5]. Series connected radial stub and shunt connected radial stubs are shown in Fig. 4.1. A

lumped equivalent circuit is given in Fig.4.2 [6], which takes into consideration the ohmic, dielectric and radiation losses in the structure. The variation of the lumped element values in the equivalent circuit with the radial stub geometry is given in Fig. 4.3 and Fig. 4.4. This representation has good agreement between theory and experiment up to the frequency corresponding to the first resonant mode of the radial structure. This frequency is given by,

$$f_x = \frac{1}{2\pi\sqrt{L_1 C_1}} \tag{4.1}$$

The agreement can be increased to higher frequencies by adding to the equivalent structure resonant cells for higher order $TM_{on}$ modes.

## 4.2 Single Stage Design:

### 4.2.1 Device Selection:

For device selection the manufacturer's data sheet was taken as a guideline. For our application the main parameter which was compared was the noise figure offered in the frequency band, 4GHz to 5GHz. The comparison of the noise figures of the devices finally chosen for testing is given in Table. 4.1. The data used for design

| Device | $NF_{min}$ | $\Gamma_{opt}$ | $R_n/50$ | Bias | |
|---|---|---|---|---|---|
| | | | | $V_{DS}(V)$ | $I_{DS}(mA)$ |
| NE 32484A | 0.32 | 0.71∠ 59 | 0.26 | 2 | 10 |
| NE 42184A | 0.40 | 0.78∠ 52 | 0.33 | 2 | 10 |
| FHX 04LG | 0.35 | 0.74∠ 31 | 0.45 | 2 | 10 |
| FHC 30FA | 0.35 | 0.73∠ 59 | 0.42 | 2 | 10 |

Table 4.1: Noise Parameters of Devices

purposes was also taken from the manufacturer's data sheet. As the reference plane for the S parameters are not specified, difference between the designed values and

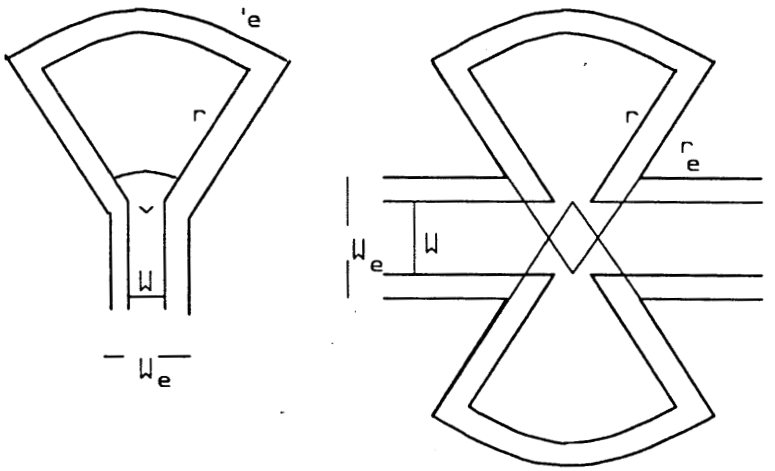


FIG. 4.1 (a) SERIES CONNECTED RADIAL STUB.
(b) SHUNT CONNECTED RADIAL STUB.

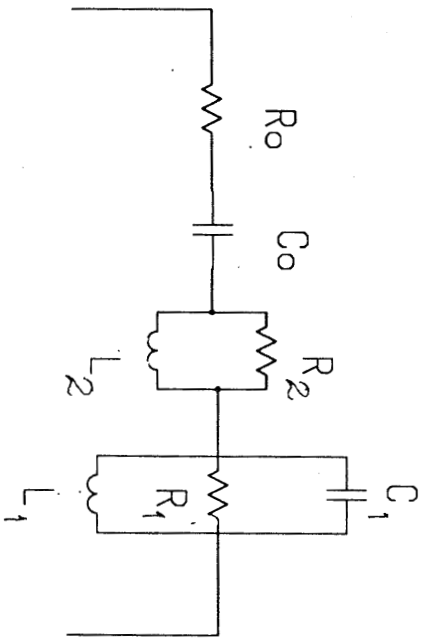


FIG. 4.2 LUMPED EQUIVALENT CIRCUIT OF RADIAL STUB[6]

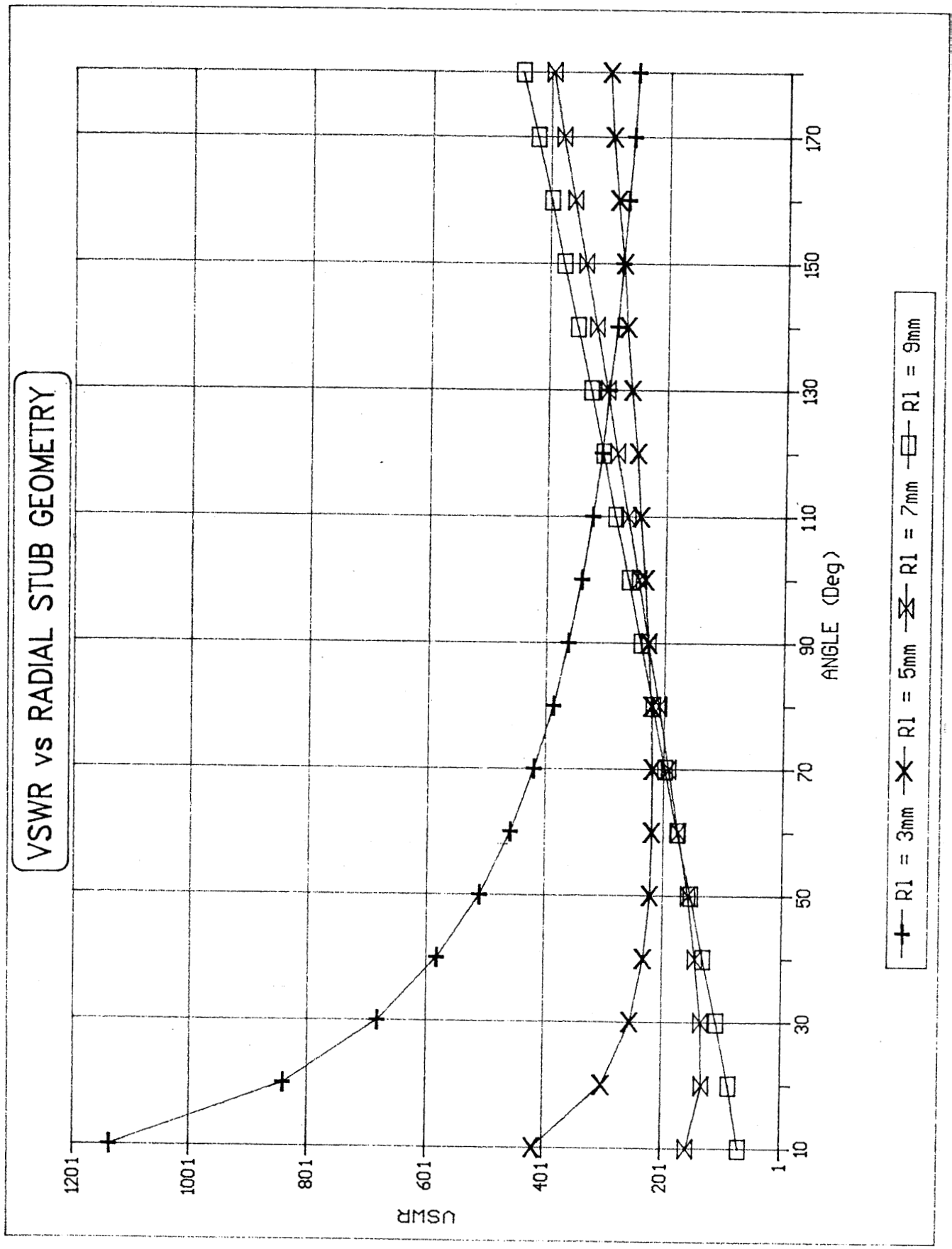
VSWR vs RADIAL STUB GEOMETRY
VSWR
1201
1001
801
601
401
201
1
10
30
50
70
90
110
130
150
170
ANGLE (Deg)
R1 = 3mm
R1 = 5mm
R1 = 7mm
R1 = 9mm

the values actually obtained is expected. The S-parameters chosen were for the minimum noise bias.

### 4.2.2 Source Feedback:

Usually for a given transistor simultaneous matching for gain and noise is not possible. As is evident from the noise and gain circles for the NEC device N32484A given in Fig.4.5a, the two do not coincide. The solution proposed is to change the input impedance, $Z_{in}$ of the transistor, so as to to be closer to the optimum input impedance for minimum noise. This can be achieved by giving inductive feedback. The equivalent circuit employed to analyze the variation in input impedance with source inductance is as in Fig.4.6. Assuming The source inductance $L_s$ to be small compared to $Y_2^{-1}$ and $Y_L^{-1}$ the input impedance $Z_{in}$ is given by,

$$Z_{in} = R_1 + j\omega L_s + \frac{1}{j\omega C_1} + \frac{L_s g_m}{C_1(1 + Y_2/\ Y_L)} + \frac{(\omega L_s)^2 Y_2}{1 + Y_2/\ Y_L} \tag{4.2}$$

It is seen that both the imaginary as well as the real part of the input impedance is affected by the feedback. Usually the value of $L_s$ is of the order of 1-2nH and the variation in the real part is more pronounced. The addition of a lossless element in the feedback path of an amplifier has been proved to have no effect on the minimum noise figure of an amplifier [7]. It has been shown by Vendelin[8] that source inductive feedback changes $Z_{opt}$ to,

$$Z'_{opt} = Z_{opt} - j\omega L_s \tag{4.3}$$

For practical values of $L_s$ this change is negligible.The variation in the noise and gain circles with an inductive feedback is given in Fig.4.5b.

### 4.2.3 Impedance Matching Circuits:

The input circuit is designed for the optimum input impedance (Zopt), minimum loss, and broad band matching. A four element matching circuit is opted for.

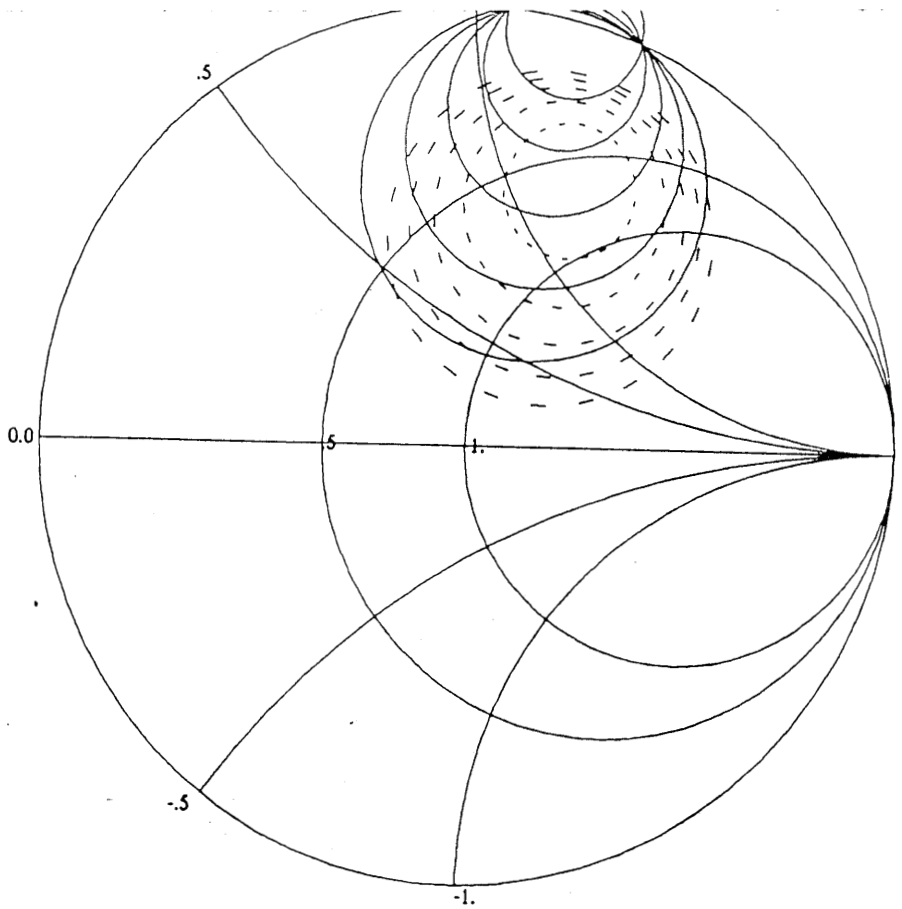


(a)

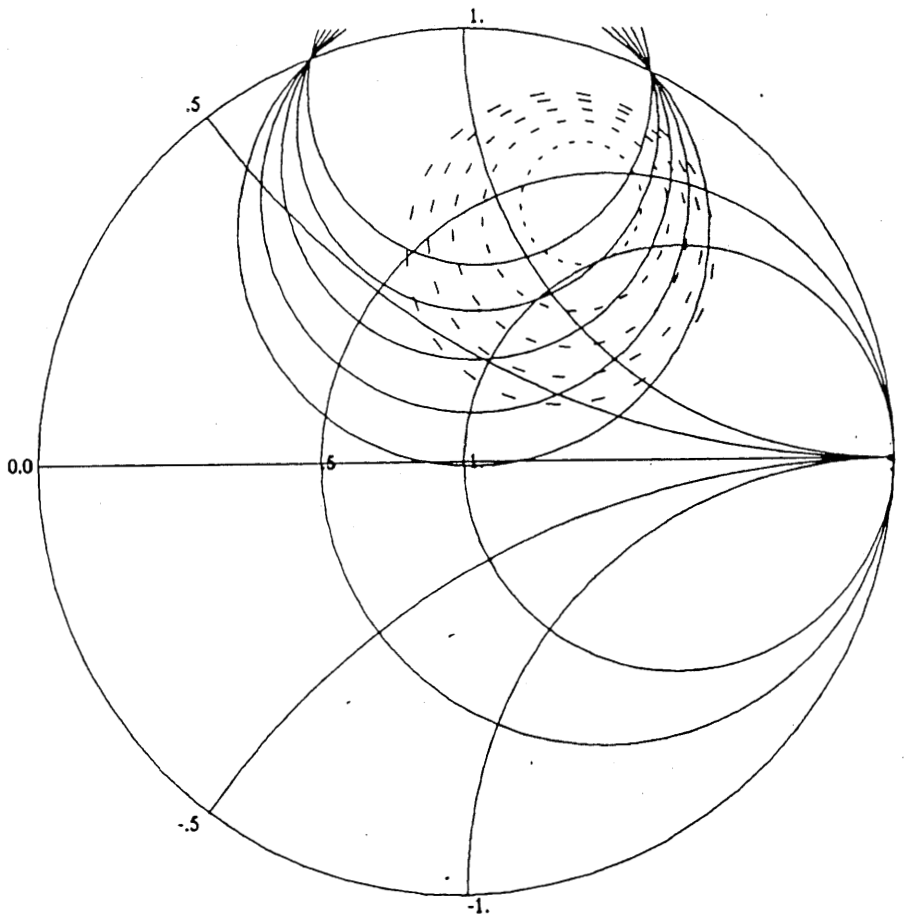


(b)

FIG. 4.5 NOISE GAIN CIRCLES OF NE32484A (a) WITHOUT FEED BACK
(b) WITH FEED BACK OF 0.2nH.

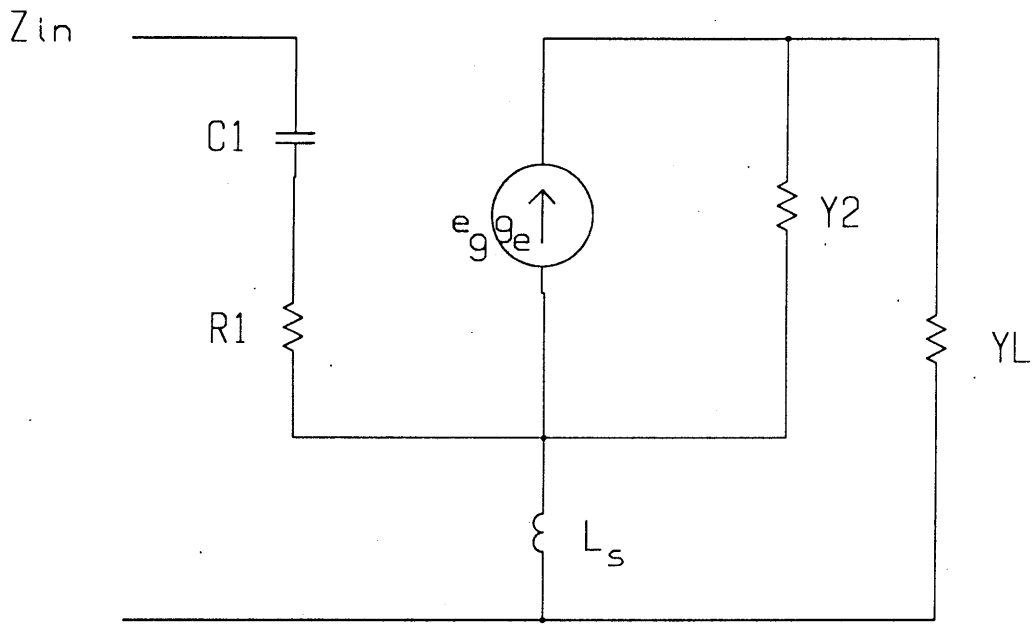


FIG. 4.6 EQUIVALENT CIRCUIT USED TO CALCULATE THE VARIATION IN INPUT IMPEDANCE WITH SOURCE INDUCTIVE FEEDBACK

The output reflection coefficients for the designed input port termination is calculated using the equation,

$$\Gamma_{OUT} = S_{22} + \frac{S_{21}S_{11}\Gamma_s}{1 - S_{11}\Gamma_s} \tag{4.4}$$

The output circuit is designed as a four element network. All the matching circuitry except the coupling capacitors were realized in microstrip .

The designed circuit is optimized for performance using Microwave Harmonica (Registerd trade mark of Compact Software), a microwave design software. During the optimization process the discontinuities like, junctions, gaps, open ends, etc are taken into consideration and analyzed.

### 4.2.4 Bias Circuit:

The transistors are actively biased using an available circuit. Any frequency components in the bias supply can result in amplifier instability. The bias isolation scheme used in the design is as shown in Fig. 4.7. The radial stub along with the 1000pF and 20pF capacitors serve to filter out any frequency components in the bias supply. It was seen that using ferrite beads in the supply line improves the stability of the circuit by effectively damping any high frequency components. The feedthrough acts as a low pass filter in the bias circuit. The feedthrough used has an insertion loss of 20dB at 10MHz.

### 4.2.5 Capacitors:

The DC blocking capacitors are the only lumped elements in the RF path other than the active device. ATC (American Tachnical Ceramics Corp., New York, U.S.A) chip capacitors are used. For minimizing the parallel resonance effects the alignment specified by the manufacturer is as shown in Fig.4.8. This has to be adhered to during assembly.

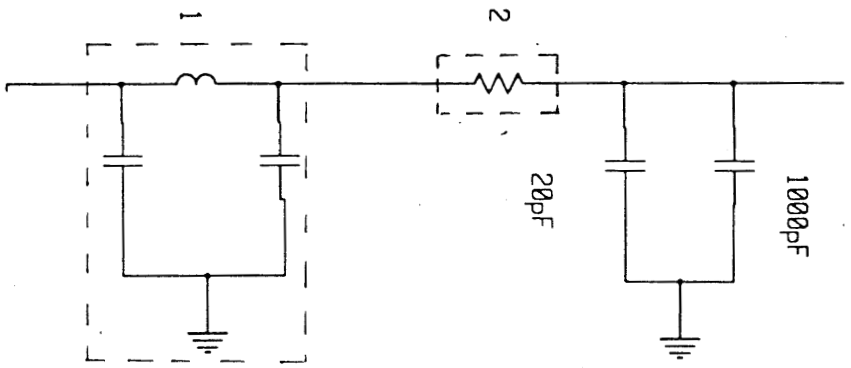


1. LOW PASS FILTER (FEED THROUGH
2. FERRITE BEAD.

P1 RADIAL STUB PRESENTS A BROAD BAND LOW IMPEDANCE POINT AT X.

P2 HIGH IMPEDENCE /4 LINE INVERTS LOW IMPEDANCE AT X TO OPEN CIRCUIT AT Y.

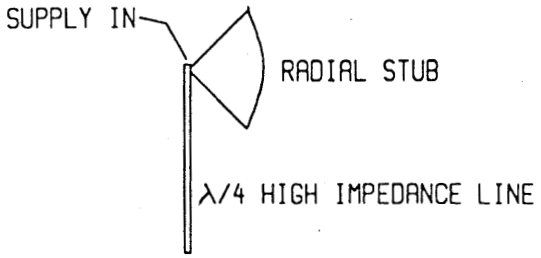


FIG. 4.7 BIAS ISOLATION CIRCUIT

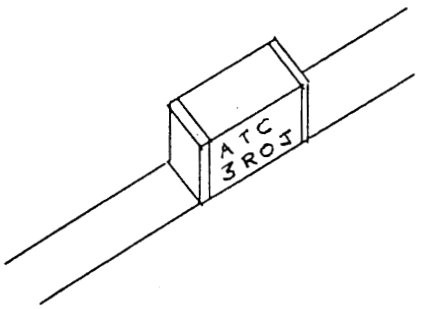


FIG. 4.8 CAPACITOR ALIGNMENT FOR MINIMIZING PARALLAL RESONANCE EFFECTS.

### 4.2.6 Board Layout:

The schematic layout and the PCB layout of the single stage are as shown in Fig.4.9. Standard photo etching procedure is followed as the accuracy required is of the order of 100 microns only.

### 4.2.7 Enclosure:

A brass chassis was opted for taking into consideration the thermal and electrical conductivities. The chassis diagram is as shown in Fig. 4.10. A gap ($\sim$ 1mm) is left on all the sides of the board so as to allow for expansion of the board during the soldering of the board to the chassis.

### 4.2.8 Device Holder:

The device holder in Fig.4.11a serves the dual purpose of maintaining the device at the chassis temperature and as a tunable inductive feedback. Maintaining the device at the chassis temperature is imperative as this design is to be modified to a cooled amplifier. The inductive feedback can be varied by changing the tab position and hence the effective grounding point.

## 4.3 Assembly:

A copper clad board with a woven glass reinforced PTFE substrate was used, whose data is given below,

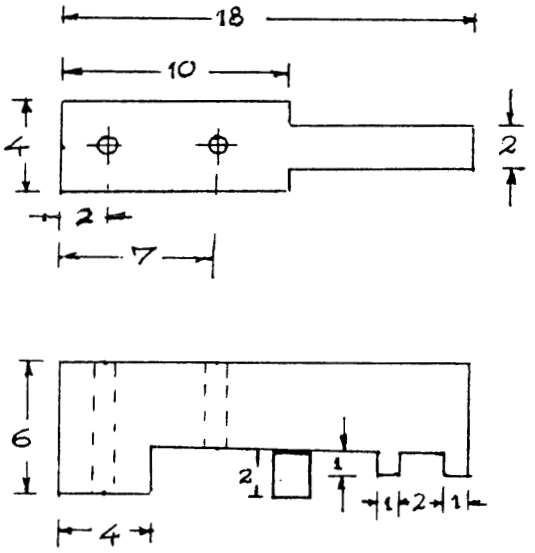


(a)

DIMENSIONS IN MM

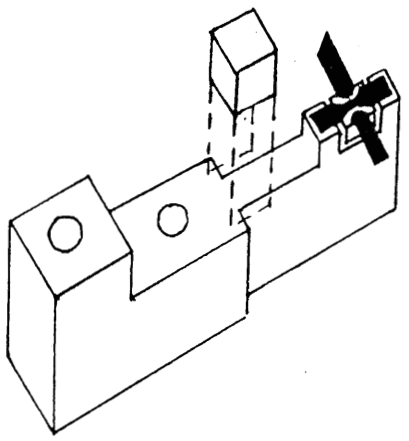

(b)

FIG. 4.11(a) DEVICE HOLDER

(b) DEVICE MOUNTING

Dielectric constant, $\epsilon_r$ $= 2.5 \pm .04$

Dissipation factor, $\tan D$ =0.0019

Substrate thickness, h =0.762mm

Metal Thickness = 20 microns

Coefficient of Thermal Expansion :

X = 9.5 ppm/$^oC$

Y = 9.5 ppm/$^oC$

Z = 120 ppm/$^oC$

The bottom of the board was soldered completely onto the chassis. For this the chassis was heated to a temperature of 200$^oC$ and solder of composition 60%Sn/40%Pb used. The transistor is soldered onto the device holder as shown in Fig.4.11b. The solder is 100% In. The temperature and time limit given by the manufacturers should not be exceeded during the soldering process. The transistor is static sensitive and sufficient precaution has to be taken while handling them. The surface of the microstrip was cleaned thoroughly with a solvent and then tinned using Sn62 (62%Sn/36%Pb/2%Ag) solder. For soldering the other components like the capacitors, chip resistors, and the input terminal Sn62 was used. This is to prevent silver leaching at the capacitor terminals. The terminals of the input and output SMA connectors should be sitting on the microstrip line so that the microstrip to coaxial transition does not present a considerable discontinuity. In the input circuit this can considerably affect the noise performance.

## 4.4 Three Stage Design:

For the three stage the experience gained from the single stage is used in the design process.

The input stage of the first transistor is designed only for the optimum source impedance, $Z_{opt}$.A double stub network is used for better bandwidth and also tuning can be done in smaller steps.

The first and second inter stages are designed for gain matching as slight noise mismatching of the second and third transistors will not affect the total noise figure appreciably.

The output stage has no matching network. Only a 10dB attenuator is used here as this will take care of the output reflection coefficient. This also improves the stability of the amplifier by ensuring that the output return loss is always negative.

The schematic layout,the board layout,and the chassis is as in Fig.4.12, 4.13. The assembly procedure is the same as followed for the single stage.

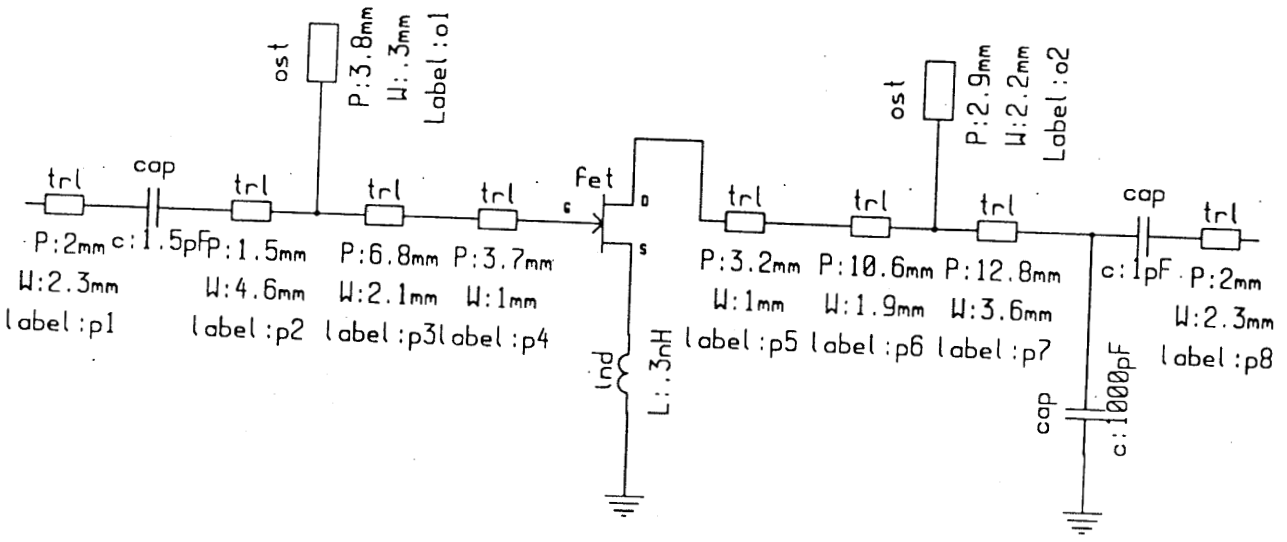


FIG.4.9a SINGLE STAGE SCHEMATIC LAYOUT

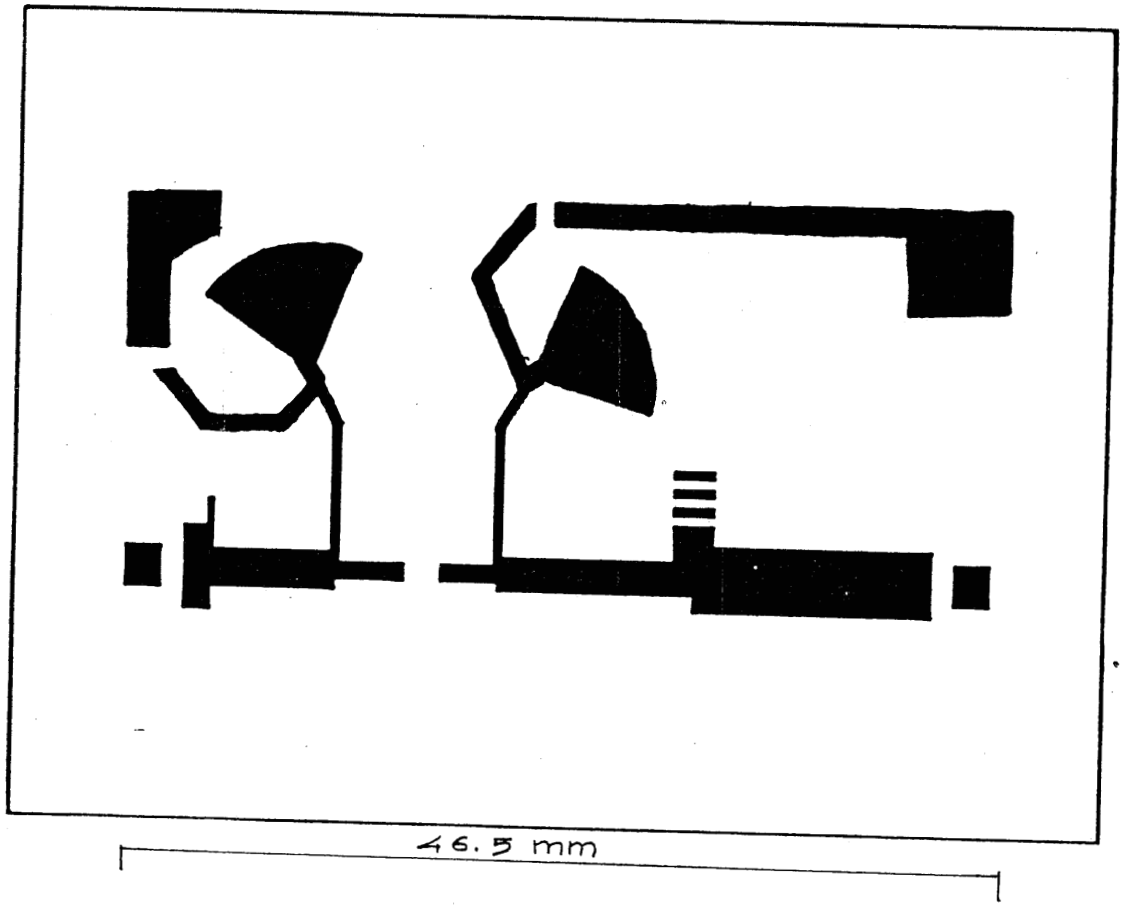


FIG. 4.9b SINGLE STAGE PCB LAYOUT.

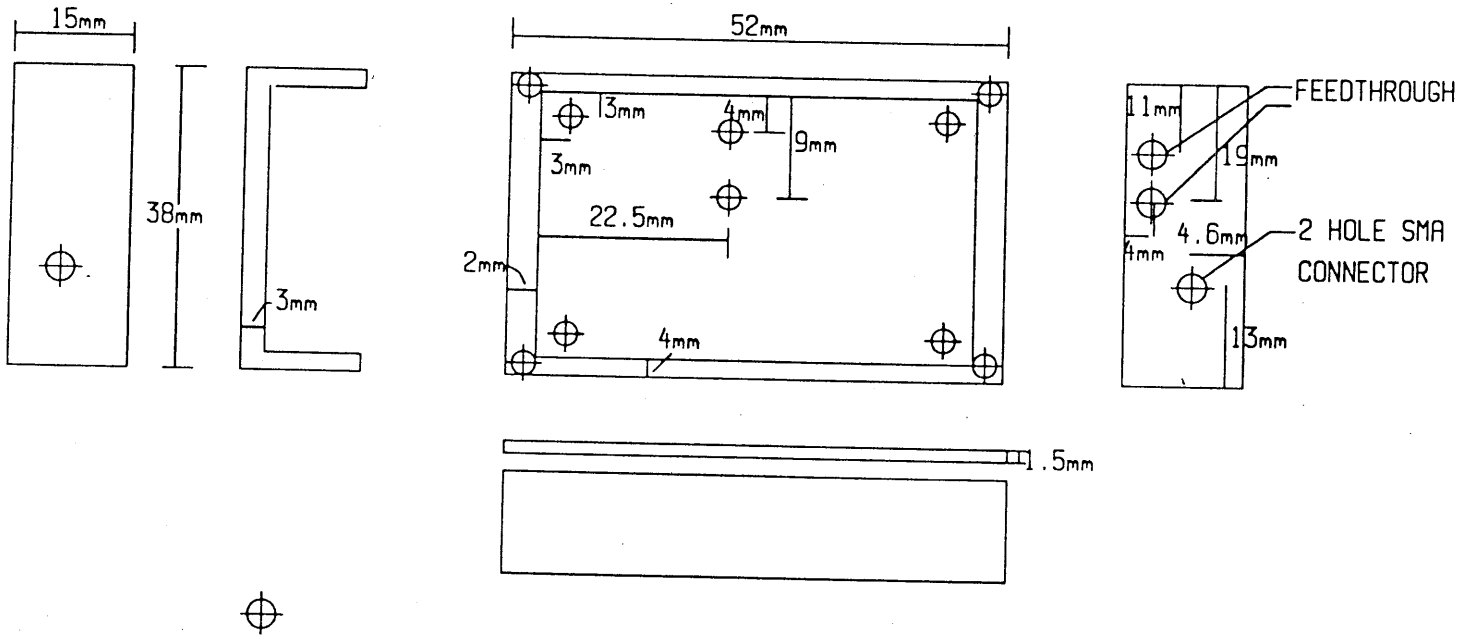


FIG. 4.10 SINGLE STAGE CHASSIS

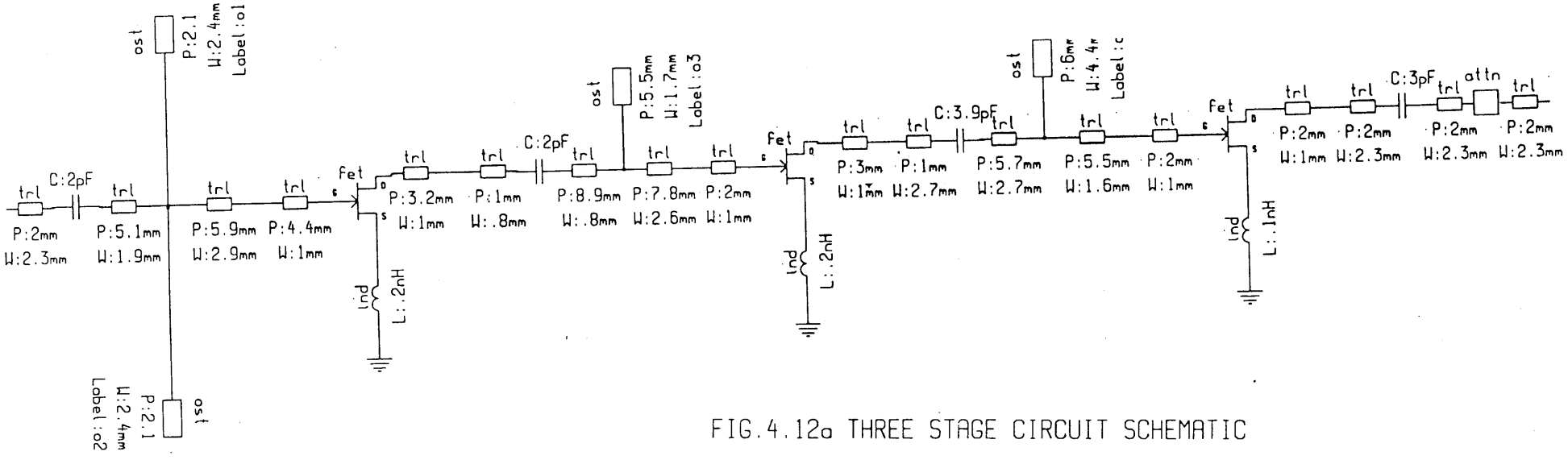


FIG.4.12a THREE STAGE CIRCUIT SCHEMATIC

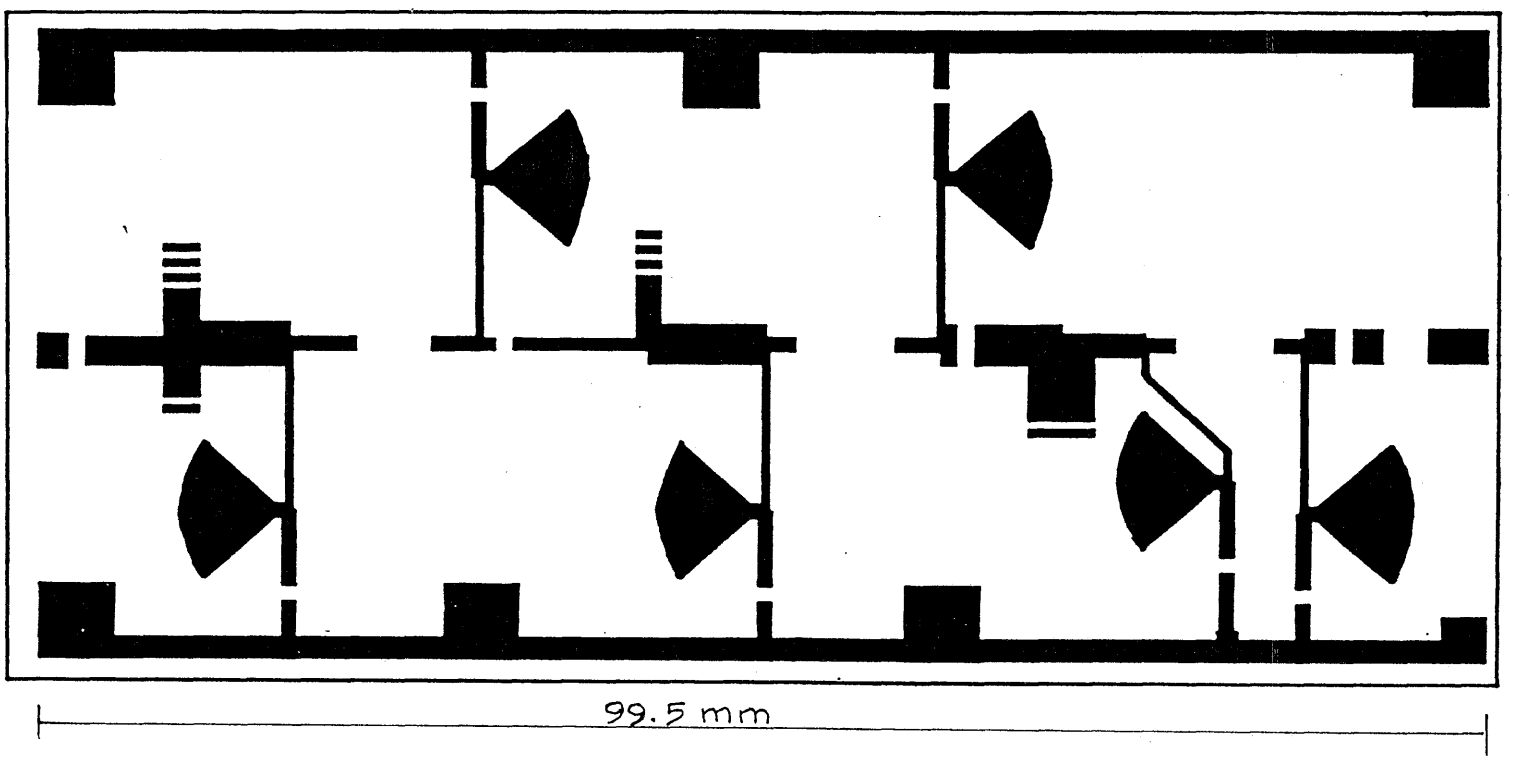


FIG. 4.12b THREE STAGE PCB LAYOUT.

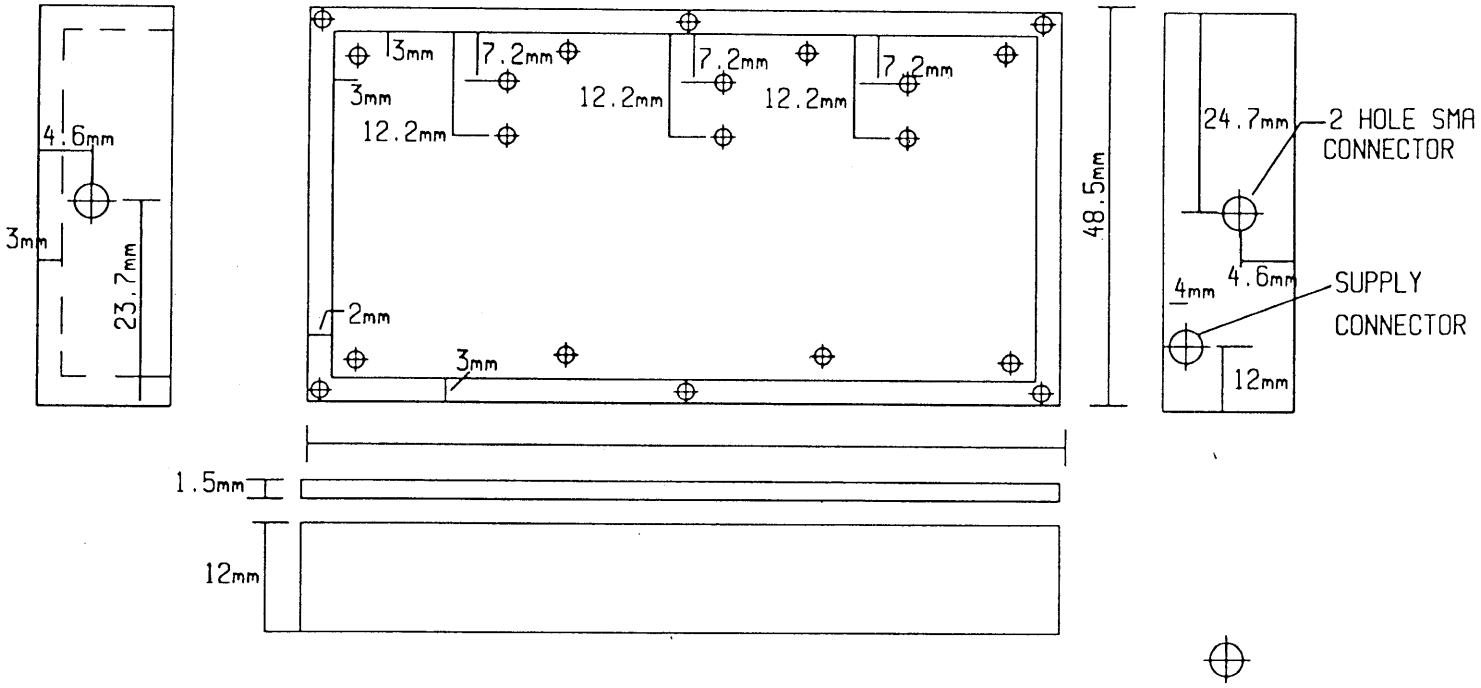


FIG. 4.13 THREE STAGE CHASSIS

# Chapter 5

# MEASUREMENT SETUP

The parameters to be measured for a LNA are:

- Stability.
- Noise Temperature
- Gain
- Input and Output return loss

## 5.1 Stability:

This is the first one to be checked. A Spectrum Analyzer is used to detect any oscillation present in the output with the input initially terminated at 50Ohms. Finally the amplifier is checked for unconditional stability with a sliding short and different resistive terminations at the input.

The spectrum analyzer used is the HP 8559A which can measure frequencies upto 26.5GHz and power levels down to -85dBm.

## 5.2 Noise Temperature and Gain:

Once the amplifier is stable with 50Ohms at the input its noise and gain performance are measured. The Eaton 2075B Noise Gain Analyzer is used.

The maximum input frequency to the Noise Gain Analyzer is 2GHz. To measure above this frequency an external down conversion has to done. The measurement set up is as shown in Fig.5.1.

The HP 8350B oscillator is controlled by the Noise Gain Analyzer. This provides the LO to the mixer.

The amplifier output is down converted to 30MHz and fed to the Noise Gain Analyzer. The IF output of the mixer is low pass filtered before being fed to the analyzer.

The system is initially calibrated without the DUT in the setup. The amplifier is included to minimize the noise contribution of the circulator and mixer. Swept frequency measurements are made.

## 5.3 Return Loss Measurement:

The Eaton Noise Gain analyzer is used for this measurement also. The setup is as shown in Fig.5.2.

For calibration, the second port of the circulator is connected to an open circuit. For the input return loss measurement, this port is connected to the input of the amplifier whose output is terminated with 50Ohms.

## 5.4 Instrument Error:

Instrument Uncertainty: Eaton Noise Gain Analyser 2075B

Noise Figure = $\pm 0.05$dB

Gain = $\pm 0.15$dB

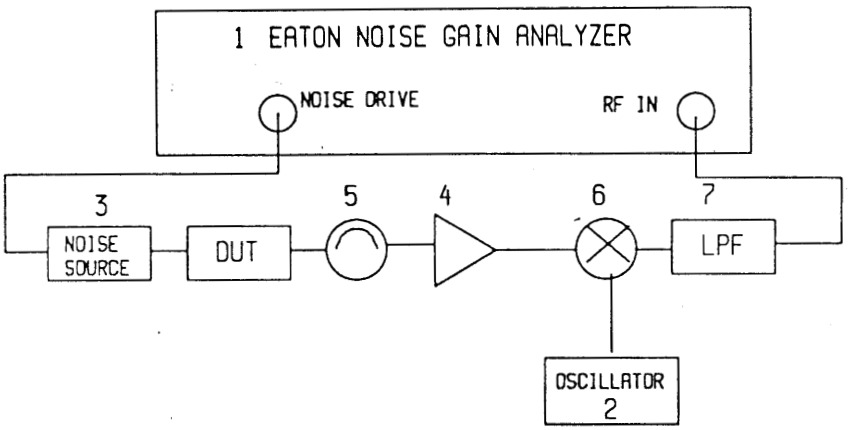


FIG. 5.1 NOISE GAIN MEASUREMENT SETUP

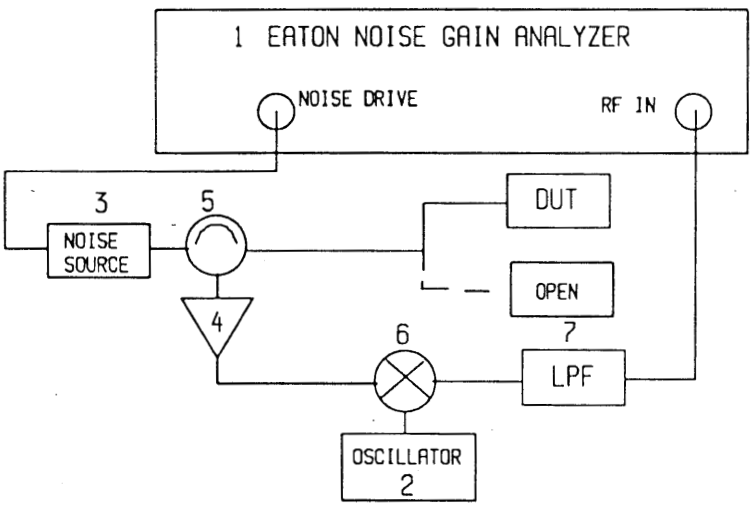


FIG. 5.2 INPUT RETURN LOSS MEASUREMENT SET UP

1. EATON Noise Gain Analyzer - 2075B

   Maximum measurable Gain = 50dB
   Input Frequency Range = 10MHz - 2GHz
   Maximum Input Power = +20dBm
   Final Detector Bandwidth 10MHz

2. Oscillator HP 8350B

   Output Frequency Range = 10MHz - 26.5GHz
   Maximum Output Power = +20dBm
   Frequency Resolution = ±5MHz

3. Noise Source HP 346A

   Frequency Range = 10MHz - 18GHz
   ENR = 4.75dB @ 4GHz
   Output VSWR = 1.1

4. Amplifier Miteq AMF 3B-4080-25

   Frequency Range = 4GHz - 8GHz
   Noise Figure = 2dB
   Maximum input VSWR = 2.3
   Maximum output VSWR = 2.0
   Gain = 25dB

5. Circulator ASC-4080

   Frequency Range = 4GHz - 8GHz
   Insertion Loss = 0.1dB
   Isolation = 30dB

6. Mixer Watkin Johnson M1J

Frequency Range RF/LO = 1.8GHz - 6.2GHz
Frequency Range IF = DC - 500MHz
Loss = 7dB

7. Low Pass Filter Lark Engg LSF800-6AA

Cut Off Frequency = 800MHz
Insertion Loss = 0.3dB

8. Spectrum Analyzer HP 8559A

Minimum Detectable Power Level = -85dBm
Frequency Range = 10MHz-26.5Ghz
Maximum Input Power = 20dBm

# Chapter 6

# RESULTS AND CONCLUSION

The testing setup described in the previous chapter was used to test the single and three stage amplifiers. The initial tuning was done with the HP8559A spectrum analyzer to suppress oscillations and the Eaton 2075 Noise Gain analyzer for the gain and noise measurements.

## 6.1 Single Stage:

The circuit which was designed for NE32484A was first checked for stability with the input terminated at 50 Ohms. Oscillations were present at a number of frequencies, which were not predicted.

Absorber sheets on the lid were seen to be helpful in suppressing the oscillations. The absorber sheets are thin silicone rubber sheet stock which has high loss at UHF and microwave frequencies. Keeping the absorber sheets over the input stage affects the noise performance adversely.

Fixing a metal tab over the device holder as shown in Fig.6.1, improves the stability. The ground post formed by this arrangement attenuates the waveguide modes.

The position of the grounding tab in the device holder was seen to affect the gain performance. The minimum position of the tab gave the best gain values. Tuning

FIG. 6.1 GROUND POST FOR WAVEGUIDE MODE ATTENUATION

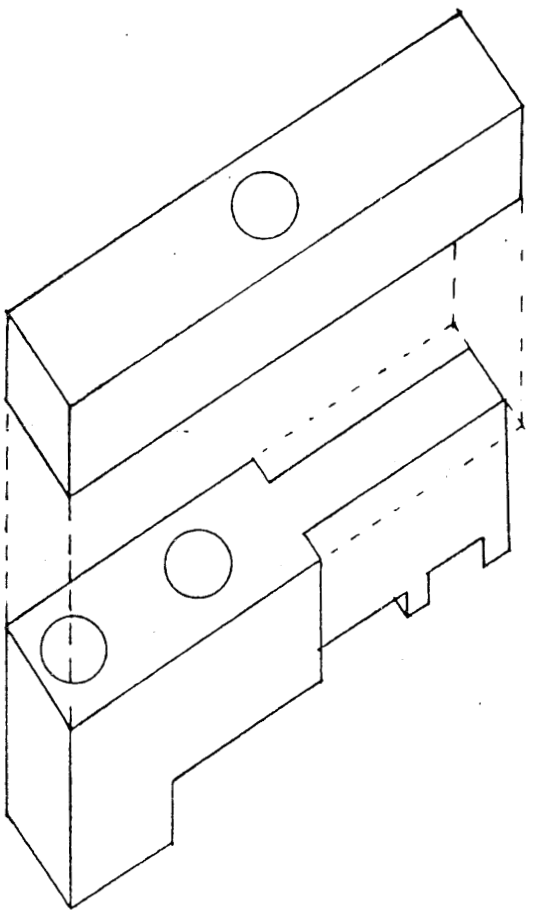

was done by changing the values of the coupling capacitors and by varying the length of the open stubs. All the possible combinations were tried out and the best values taken. As the $Z_{opt}$ of the different devices are close it was possible to check the noise performance of the different devices in the same circuit. Tuning was done for each transistor. The performance of the different devices are given. FHC30FA is seen to give the best noise performance in this circuit. The amplifier is conditionally stable.

## 6.2 Three Stage:

The three stage was tested with NE32484A in the first stage and NE42184A in the second and third stages. Absorber sheets and ground posts are used to kill oscillations as in the single stage.

Tuning was done by varying the coupling capacitors and the length of the open stubs. The gain and noise performance was not satisfactory.

Different combinations of the devices were tried. The best results were obtained with NE32484A in the first and second stages and NE42184A in the third stage. The results are as shown. The amplifier is conditionally stable. The high gain makes stabilizing the amplifier a difficult task especially with limited tuning elements.

## 6.3 Conclusion:

The designed values vary from the measured ones. This could be because of the variation in S-parameters of the transistors from even the same batch and the circuit parasitics not modelled. S-parameter characterization has to be done for each transistor.

The amplifier gives a 3dB gain bandwidth of 1GHz and less than 50K noise temperature over the same band. The amplifier has to be made unconditionally stable. The circuit can be optimized further.

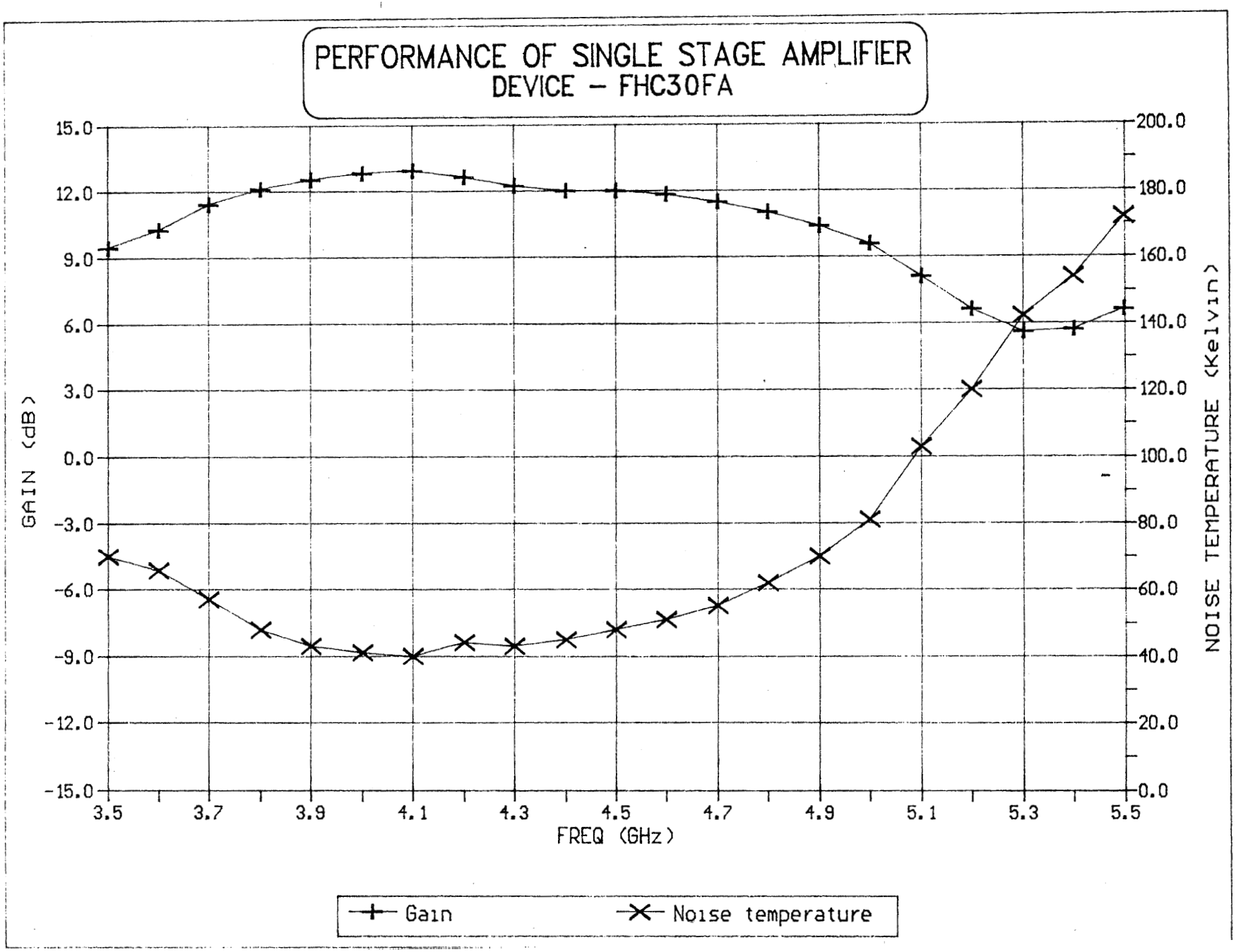
PERFORMANCE OF SINGLE STAGE AMPLIFIER
DEVICE – FHC30FA
GAIN (dB)
15.0
12.0
9.0
6.0
3.0
0.0
-3.0
-6.0
-9.0
-12.0
-15.0
NOISE TEMPERATURE (Kelvin)
200.0
180.0
160.0
140.0
120.0
100.0
80.0
60.0
40.0
20.0
0.0
3.5
3.7
3.9
4.1
4.3
4.5
4.7
4.9
5.1
5.3
5.5
FREQ (GHz)
Gain
Noise temperature

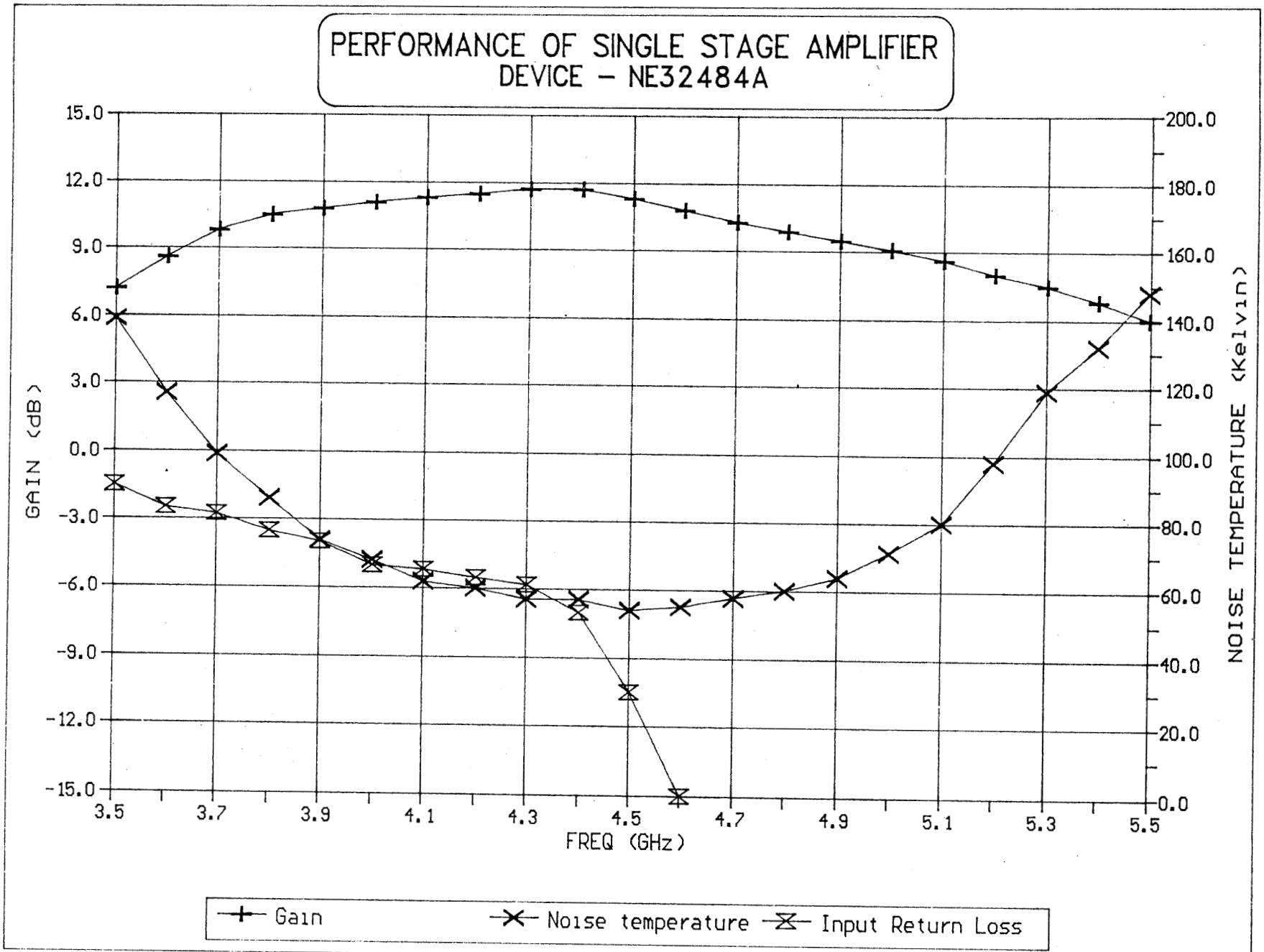
PERFORMANCE OF SINGLE STAGE AMPLIFIER
DEVICE – NE32484A
GAIN (dB)
NOISE TEMPERATURE (Kelvin)
FREQ (GHz)
15.0
12.0
9.0
6.0
3.0
0.0
-3.0
-6.0
-9.0
-12.0
-15.0
200.0
180.0
160.0
140.0
120.0
100.0
80.0
60.0
40.0
20.0
0.0
3.5
3.7
3.9
4.1
4.3
4.5
4.7
4.9
5.1
5.3
5.5
Gain
Noise temperature
Input Return Loss

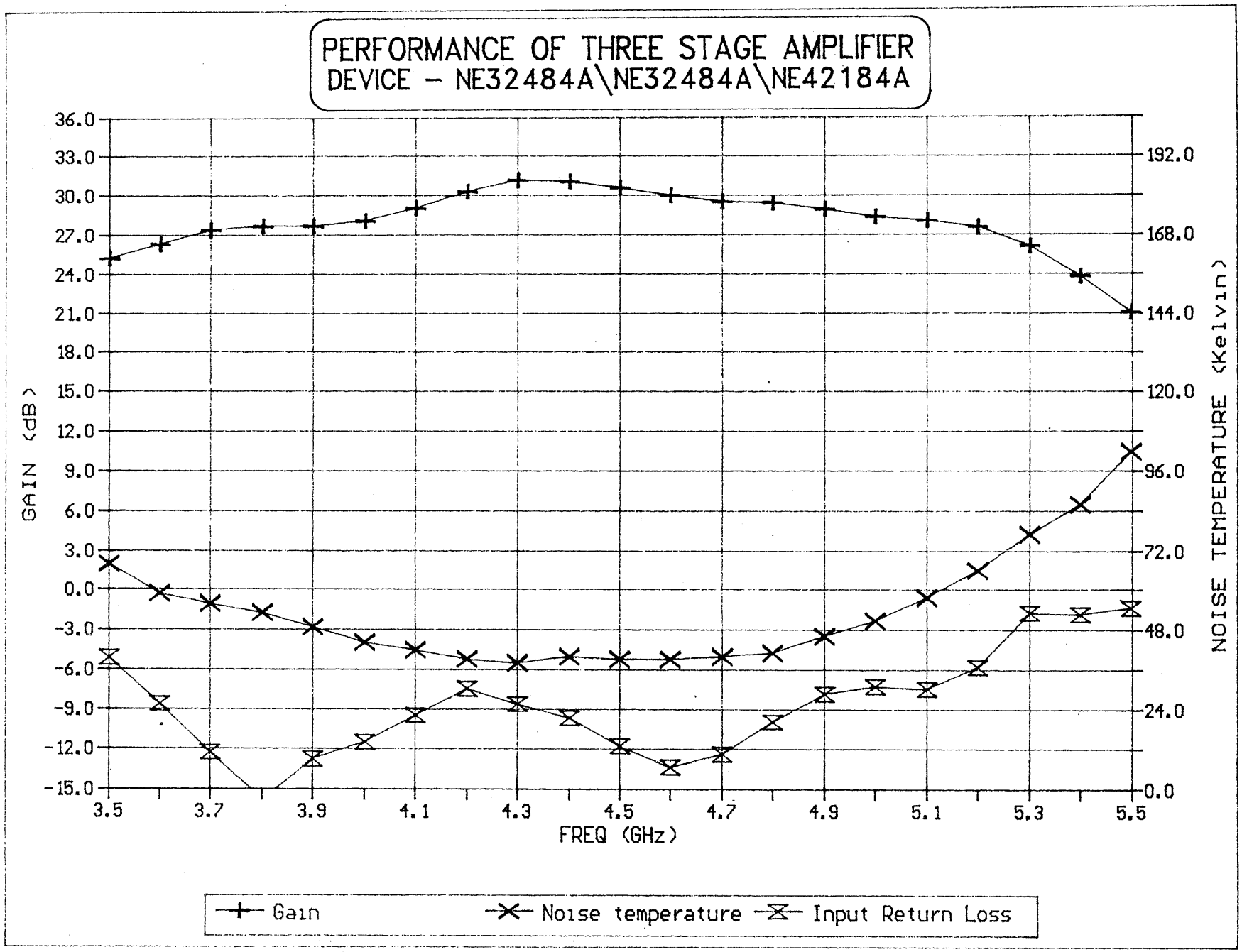
PERFORMANCE OF THREE STAGE AMPLIFIER
DEVICE – NE32484A\NE32484A\NE42184A
GAIN (dB)
36.0
33.0
30.0
27.0
24.0
21.0
18.0
15.0
12.0
9.0
6.0
3.0
0.0
-3.0
-6.0
-9.0
-12.0
-15.0
NOISE TEMPERATURE (Kelvin)
192.0
168.0
144.0
120.0
96.0
72.0
48.0
24.0
0.0
3.5
3.7
3.9
4.1
4.3
4.5
4.7
4.9
5.1
5.3
5.5
FREQ (GHz)
Gain
Noise temperature
Input Return Loss

# Bibliography


[1] Kraus, John, D.,: *Radio Astronomy*, McGraw Hill Book company, U.S.A., 1966.

[2] Roger, D., P.,: *Microwave network characterization*, Leeds University Press, England, 1989.

[3] Dingle, R., *et al*: *Electron Mobilities in Modulation Doped Superlattices*, App. Physics Letters, October 1978.

[4] Asu, R., J.,: *Parametric Analysis for a Millimeter Wave Low Noise HEMT*, Int. Journal of Infrared and Millimeter Waves, Vol.9, 1988.

[5] Giannini, F., Sorrentino, R., Vrba, J., : *Planar circuit analysis of microstrip radial stub*, IEEE Trans. Microwave Theory Tech., Vol. MTT32, December 1984.

[6] Giannini, F., Paoloni, C., and Ruggieri, M., : *CAD oriented lossy models for radial stubs*, IEEE Trans. Microwave Theory Tech., MTT36, February 1988.

[7] Haus, H., and Adler, R., : *Optimum noise performance of linear amplifiers*, Proc. IRE, Vol.46, August 1958.

[8] Vendelin, G., : *Feedback effects on the noise performance of GaAs MESFETs*, Int. Microwave Symp., Dig. Tech. Papers, 1975.

[9] Edvards, Terry, : *Foundations for microstrip circuit design*,John Wiley and sons, England, 1992.

[10] Chang, Kai, : *Handbook of microwave and optical components*, John Wiley and sons, New York, 1990.

[11] Raymond, S., P.,: *Amplifiers*, Leeds University Press, England, 1989.

[12] Gonzalez, G.,: *Microwave Transistor Amplifiers*, Prentice- Hall Inc., New Jersey, 1984.